UNIVERSITY OF SHEFFIELD

department of chemical engineering and fuel technology

FUNDAMENTAL STUDY OF THREE DIMENSIONAL
TWO PHASE FLOW IN COMBUSTION
SYSTEMS

J. SWITHENBANK, B.C.R. EWAN,
F. BOYSAN, W.H. AYERS
S.V. MALEBRAN

FINAL REPORT JUNE 1983

REPORT DOCUMENTATION PAGE		BEFORE COMPLETING FORM
1. REPORT NUMBER	2. GOVT ACCESSION NO. AD-A142886	3. RECIPIENT'S CATALOG NUMBER
4. TITLE (and Subtitle) FUNDAMENTAL STUDY OF THREE DIMENSIONAL TWO PHASE FLOW IN COMBUSTION SYSTEMS		5. TYPE OF REPORT & PERIOD COVERED FINAL REPORT TO JUNE 1983
		6. PERFORMING ORG. REPORT NUMBER
7. AUTHOR(s) PROF. J. SWITHENBANK, B.C.R.EWAN, F.BOYSAN, W.H.AYERS		8. CONTRACT OR GRANT NUMBER(s) AFOSR - 82 - 0272
9. PERFORMING ORGANIZATION NAME AND ADDRESS Dept. of Chemical Eng. & Fuel Technology University of Sheffield, Mappin Street, Sheffield S1 3JD, England		10. PROGRAM ELEMENT, PROJECT, TASK AREA & WORK UNIT NUMBERS 2308 - A2
11. CONTROLLING OFFICE NAME AND ADDRESS AFOSR/NA, Building 410, Bolling Air Force Base D.C. 20332		12. REPORT DATE 20th Dec. 1983
		13. NUMBER OF PAGES 78
14. MONITORING AGENCY NAME & ADDRESS(if different from Controlling Office) EOARD, 223 Old Marleybone Road London NW1 5TH, England		15. SECURITY CLASS. (of this report)
		15a. DECLASSIFICATION/DOWNGRADING SCHEDULE

16. DISTRIBUTION STATEMENT (of this Report)

CLEARED FOR PUBLIC RELEASE

17. DISTRIBUTION STATEMENT (of the abstract entered in Block 20, if different from Report)

18. SUPPLEMENTARY NOTES

19. KEY WORDS (Continue on reverse side if necessary and identify by block number)

COMBUSTION MODELLING, TURBULENCE MODELLING, DUMP COMBUSTOR
SWIRLING FLOW

20. ABSTRACT (Continue on reverse side if necessary and identify by block number)

Details are presented on the latest developments in the mathematical modelling of turbulence with particular reference to the pressure strain transport term. Comparisons are made of the radial variation of normal and shear stress with published data for a round jet and for decay of turbulence for selected flow fields. Work is also reported on the measurement and calculation of flow fields inside a dump combustor using swirl and baffle stabilisation. The value of the different turbulence approximations in predicting the flow are discussed.

DD FORM 1 JAN 73 1473 EDITION OF 1 NOV 65 IS OBSOLETE

SECURITY CLASSIFICATION OF THIS PAGE (When Data Entered)

Grant Number: AFOSR - 82 - 0272

FUNDAMENTAL STUDY OF THREE DIMENSIONAL TWO PHASE FLOW IN COMBUSTION SYSTEMS

Prof. J. Swithenbank
Department of Chemical Engineering
& Fuel Technology
University of Sheffield
England

20th December 1983

Final Report, for the period up to June 1983

Approved for public release
distribution unlimited

Prepared for AFOSR/NA
Building 410
Bolling AFB
D.C.20332

and

EUROPEAN OFFICE OF AEROSPACE RESEARCH AND DEVELOPMENT
London, England

Introduction

The overall objective of this program has been to carry out fundamental research to support a continuing design program for combustors of interest to USAF.

This goal is one which has many contributing elements, and of necessity, the emphasis of the work in any one period has moved to address the most relevant aspects of the problem. In broad terms these have been seen to be :-

1. The refinement of the individual models which contribute to the overall finite difference combustion algorithm. These include particularly kinetics, fuel preparation and evaporation and the radiation flux contribution to enthalpy.
2. The fundamental analysis of an adequate turbulence representation.
3. Research into efficient iterative procedures.
4. To study the possibilities for interactive software suitable for non-expert usage.
5. Carrying out of measurements to validate models.

The following review describes the progress made in recent years in each of these areas and emphasises the most important areas for future work.

Review of Recent Progress

Combustion Modelling

Fuel preparation, evaporation and mixing are of central importance to any combustion model.

The evaporation problem was first approached from the viewpoint of individual droplets by considering the trajectories of droplets through a given combustor flow field based on suitable droplet drag and evaporation laws applied to each finite difference cell.

This was followed by an extension to three dimensions and the integration of both Lagrangian and Eulerian solution procedures for droplets and flow fields into an iterative scheme. This enabled one to observe the fate of individual droplet size groups for a particular combustor geometry, and results were presented for hot and cold flow fields for a gas turbine can, demonstrating different droplet trajectory patterns for different spray cone angles.

It thus became possible to match nozzle type with combustors since unevaporated droplets escaping from the combustor could be monitored for unsuitable nozzles. This has been seen as an important achievement and

has generated interest from several quarters including Parker-Hannefin, Lycoming and Pratt & Whitney.

Following the earlier developments, the interaction of droplets and flow is now fully coupled in both directions. In addition, the influence of turbulence on droplet motion is incorporated by applying a randomised turbulent contribution to the mean flow velocity in each cell, based on local turbulence intensity and a random variable. This is important in representing the spread of droplets in low mixing regions.

An optimised iterative scheme for the combustion case is summarised as follows -

i) The u,v,w momentum equations are each solved in turn using guessed pressures

ii) Since the velocities do not satisfy the mass continuity equation locally, a "Poisson type" equation is derived from the continuity equation and the three linearised momentum equations. This pressure correction equation is then solved to obtain the necessary corrections to the pressure field and corresponding adjustments to the velocity components are made.

iii) The k and ϵ equations are solved using the updated velocity field to obtain the distribution of effective viscosity.

iv) Any auxiliary equations (e.g. enthalpy, species, conservation, radiation or turbulence properties) are solved using the previously updated values of the other variables.

v) Where interphase coupling is to be included, a solution of the equations of motion of the droplets is obtained at intervals and used to augment the source terms of the appropriate gas flow equations.

These steps can be continued until the error mentioned in (ii) has decreased to the required value.

Turbulence Modelling

It has been seen as important that the approach to the turbulence representation be of a fundamental nature in order that the model be applicable to a wide range of geometries. The problem revolves around the representation of the Reynolds stress components and the various options which are commonly available in turbulence modelling are shown in Figure 1.

These broadly divide between effective viscosity models and fundamental models. In the former, the individual stresses are related to an isotropic turbulence viscosity field. This in turn is related to individual turbulence parameters such as kinetic energy k and dissipation rate ϵ in the

$k - \varepsilon$ model, which are solved from their respective transport equations. For low swirl cases, the $k - \varepsilon$ model has been modified in the past by reducing the effective viscosity for stresses involving the swirl component. This was found however to have only limited success and the more fundamental option detailed in Figure 1 has been pursued at length.

Much of the development work on turbulence has been made with reference to simple swirling flows such as cyclone flows. One of the most striking demonstrations of the shortcomings of the $k - \varepsilon$ model was shown in these flows in which the reverse axial flow on the axis is not represented. It was also shown that by contrast, the algebraic model represented quite closely both the mean flow contour and the turbulence throughout the cyclone. This geometry is a fairly simple one mathematically since the axial derivatives are small and in some cases can be neglected. For more complicated flows, such as dump combustors with swirl, more solution space and time is required. The above results however , have been very rewarding for the considerable effort expended and have indicated strongly the direction in which combustion model development must proceed if the representation of swirl geometries mathematically is to be adequate.

Interactive Software

An important part of any intricate design problem is the need to be able to interact with the software both for problem definition and during calculation.

A parallel development procedure has therefore been undertaken to ensure that problems can be set up in a matter of hours and that there is easy access during runtime to monitor and change variables.

This is best illustrated with reference to Figure 2.

Combustor geometries are not defined analytically but rather by the choice of definition of each of the cells in the finite difference grid. This is a simple matter of assigning letters to each cell and some options include W for wall, I for inlet, O for outlet etc. An arbitrary geometry can thus be built up. The program also provides a list of options at each stage as well as a HELP command, which can be used at any point, to help the inexperienced user.

Experimental Measurements

These have mainly been concerned with the validation of particular aspects of model refinement and are complementary to data used from the literature. They consist of the measurement of temperature profiles to compare with the predictions of the combustion algorithm, residence time functions and velocity profiles to compare with the predictions of the mean flow and turbulence models.

In the residence time study, a short pulse of mercury vapour (1 msec) was used as tracer in a gas turbine can and monitored at the exit. By different choice of input location, the different stirred and plug flow sections could be studied. In itself, this is a quick and useful method of assessing reactor volumes and blow off performance.

Results however, were compared with mixing predictions for the $k - \varepsilon$ model using the randomised bubble tracking procedure developed for particles and referred to above. Of the five input locations studied, good agreement was obtained for the downstream positions with regard to shape and position of the response function. For the upstream input positions, good agreement with shape was obtained, indicating that the mixing volume is well represented in the model. A slight discrepancy in plug flow times for upstream input was thought to be due to some computational trapped volume on the symmetry axis of the combustor.

The method has proved a useful one in enabling a comparison to be made with predictions at the fundamental mixing level.

The measurement of flow velocity profiles using LDA has been carried out in conjunction with the turbulence model development and has been necessary since little experimental data existed for the simple swirl flows which the development program required.

For this purpose, two types of tangential entry cyclones have been measured and the present good agreement, which the algebraic turbulence model has provided has already been reported.

Progress during 1982-83

The objectives of the past year have sought to address the particular problems of swirling flows with reference to their application in dump combustors and may be itemised as follows :

1) Further development of the Sheffield algebraic turbulence model with particular reference to the pressure strain term, the role of which is to transfer energy between the different fluctuating velocity components tending to equalise the normal Reynolds stresses and decrease the absolute value of the shear stresses.
2) To investigate the effects of different types of swirl on the velocity field in a dump combustor. Swirl types would range from free vortex type to solid body.

   Investigations would include -

   a) application of a number of flow model approximations to the different types of isothermal flow to confirm the regimes of agreement and difference.

b) application of laser Doppler anemometry to determine the flow fields in the dump combustor for the different swirl types.

The following is a review of the work carried out in each of these areas and begins with a description of the turbulence modelling.

REPORT ON THE MODELLING OF THE PRESSURE INTERACTION TERM

Sergio Vasquez Malebran
Department of Chemical Engineering and Fuel Technology, Sheffield University.

Abstract

This report investigates the effects of the non-linearities on the quasi-isotropic model for pressure-strain in the Reynolds stress equation. In particular Rotta's linear return to isotropy model has been replaced by an expression which also contains the second invariant of the anisotropy tensor and a quadratic term for the Reynolds stresses. The constribution of the mean strain to the pressure interactions is modelled according to Launder, Reece and Rodi (1975) and a complete expression of the fourth order tensor is considered. A simplified version of this model is also studied where the parameter c_2 of the standard LRR model is made a function of the invariants of the anisotropy tensor. Constants resulting from the approximate expressions are adjusted in reference to homogeneous turbulent flows and satisfactory agreement was obtained for a single set of constants.

1. Introduction

The main problem in predicting turbulent flows is to determine the Reynolds stresses, $\langle u_i u_j \rangle$ which appear in the equations of conservation of momentum. Attempts have been in the past to evaluate these stresses by relating them to known or calculable quantities such as the mean velocity gradients. A simple expression of this type which is applicable to situations in which there is a single dominant direction of flow is

$$-\langle u_1 u_2 \rangle = \nu_t \frac{\partial U_1}{\partial x_2} \qquad (1)$$

where $\frac{\partial U_1}{\partial x_2}$ is the only non-zero mean velocity gradient, u is the

fluctuating velocity and ν_t is the so called eddy-viscocity. For more complex flows this simple relation can be generalized in the following fashion

$$-\langle u_i u_j \rangle = \nu_t \left(\frac{\partial U_i}{\partial x_j} + \frac{\partial U_j}{\partial x_i}\right) - \frac{2}{3} k \delta_{ij} \qquad (2)$$

where $k=\frac{1}{2}\langle u_i u_j \rangle$ is the turbulent kinetic energy. The second term on the right hand side has been added to make eq.(2) contract properly. Unlike the molecular viscocity , which is a property of the fluid, the eddy viscocity is a property of the flow and many hypotheses have so far been proposed for its evaluation. According to the Prandtl-Kolmogorov hypothesis, the eddy viscocity can be expressed as

$$\nu_t = C_\mu k^{\frac{1}{2}} l \qquad (3)$$

where k denotes the turbulent kinetic energy, l a length scale proportional to that of the energy containing motions and C_μ is a constant of proportionality. For relatively simple flows where only one Reynolds stress component is of importance, equations (2) and (3) give fairly good results. For flows where several components of the Reynolds stresses are of importance, experiments have shown that ν_t can be strongly direction sensitive. Furthemore, the empirical coefficient C_μ can no longer be regarded as a constant. Thus , the turbulence models based on the eddy viscocity concept which is expressed in equation (2) and

(3) do not produce the universality required for the calculation of complex three dimensional flows.

The governing equations of the transport of the Reynolds stresses can be derived from the Navier-Stokes equations and can be expressed in the following way:

$$\frac{D\langle u_i u_j\rangle}{Dt} = -\left[\langle u_i u_k\rangle\frac{\partial U_j}{\partial x_k} + \langle u_j u_k\rangle\frac{\partial U_i}{\partial x_k}\right] - \frac{\partial}{\partial x_k}\langle u_i u_j u_k\rangle - \frac{1}{\rho}\left\langle u_i\frac{\partial p}{\partial x_j} + u_j\frac{\partial p}{\partial x_i}\right\rangle$$

$$+ \nu\left\langle u_i\frac{\partial^2 u_j}{\partial^2 x_k} + u_j\frac{\partial^2 u_i}{\partial^2 x_k}\right\rangle \qquad (4)$$

where upper and lower case u's refer to mean and fluctuating velocity components respectively, p is the pressure, x's are the cartesian space coordinates, ν and ρ are the kinematic viscocity and the density of the fluid.The physical meaning of these terms is similar to that of the corresponding terms of the equation for the turbulent kinetic energy obtained by contracting (4); the term on the left hand side represents the convection of the Reynolds stresses (C_{ij}) while the ones on the right hand side are the production term (P_{ij}) which represents the exchange of energy from the mean motion to the turbulent motion, the dissipation term (Δ_{ij}) which expresses the diffusive transport of the Reynolds stresses, the pressure interaction term (ϕ_{ij}) which represents the correlation between velocity fluctuation and the pressure gradient, and finally the viscous dissipation term (ε_{ij}) . The

last three terms require modelling assumptions in order to relate them to known or calculable quantities. The modelling assumptions, however, are much less restrictive in this case than they are in the case of the general eddy viscocity hypothesis and the models based on the above transport equation are likely to possess a much greater potential for predicting complex flows successfully. Equation (4) is in fact a set of differential equations for the individual Reynold stress components and the solution of this set of partial differential equations, which of necessity is a numerical one, can be very expensive in terms of computing time.

2. Approximated expressions

2.1 Dissipation Term

The simplest model for the dissipation term in eq.(4) is given by

$$2\nu\left\langle \frac{\partial u_i}{\partial x_k}\frac{\partial u_j}{\partial x_k} \right\rangle = \frac{2}{3}\varepsilon\delta_{ij} \qquad (5)$$

where

$$\varepsilon = \nu\left\langle \left(\frac{\partial u_i}{\partial x_1}\right)\left(\frac{\partial u_i}{\partial x_1}\right) \right\rangle$$

This expression holds only when the dissipative motions are

isotropic and should be applicable to those flow regions where the local turbulence Reynolds numbers are high. Although experimental studies have shown that turbulence does not remain locally isotropic in the presence of strong strain fields, this expression has been used in previous modelling efforts with reasonable success.

2.2 The Diffusion Term

Although the requirement of high Reynolds numbers permits the viscous diffusion term in eq.(4) to be neglected, it is not possible to dismiss the remaining diffusion terms with confidence. Hanjalic and Launder (1972) suggest that the 'pressure diffusion' terms may also be neglected. Although their assumption is based on a single result, in the absence of any other firm evidence, this seems to be the best hypothesis. thus only the triple velocity correlations may be replaced by an expression containing only the second order correlations in the following way:

$$-\langle u_i u_j u_k \rangle = c_s' \frac{k}{\varepsilon} \left(\langle u_i u_j \rangle \frac{\partial \langle u_j u_k \rangle}{\partial x_l} + \langle u_j u_l \rangle \frac{\partial \langle u_k u_i \rangle}{\partial x_l} + \langle u_k u_l \rangle \frac{\partial \langle u_i u_j \rangle}{\partial x_l} \right) \quad (6)$$

where c_s' is a constant. A simpler gradient diffusion hypothesis has been proposed by Daly and Harlow (1970) which is expressed as:

$$-\langle u_i u_j u_k \rangle = c_s \frac{k}{\varepsilon} \langle u_k u_l \rangle \frac{\partial \langle u_i u_j \rangle}{\partial x_l} \qquad (7)$$

where c_s is a constant. Launder Reece and Rodi (1975) suggest that the constants c_s' and c_s take the values of 0.11 and 0.22 respectively.

2.3 Pressure Interaction Term

for mod ling purposes the pressure interaction term is often split into a sum of two components

$$-\left\langle \frac{1}{\rho}\left(u_j \frac{\partial p}{\partial x_i} + u_i \frac{\partial p}{\partial x_j}\right)\right\rangle = \left\langle \frac{p}{\rho}\left(\frac{\partial u_i}{\partial x_j} + \frac{\partial u_j}{\partial x_i}\right)\right\rangle - \left\langle \frac{1}{\rho}\left(\frac{\partial}{\partial x_i}(pu_j) + \frac{\partial}{\partial x_j}(pu_i)\right)\right\rangle \qquad (8)$$

where the first term on the right hand side is the pressure-strain correlation and since its trace vanishes its role is to transfer energy among components and not to create or destroy it. The second term is referred as the 'pressure diffusion' and it is usually neglected in the modelling procedures.

Following Chou (1945), the explicit appearance of the pressure fluctuation satisfies the following Poisson's equation:

$$\frac{1}{\rho}\frac{\partial^2 p}{\partial x_i \partial x_i} = \frac{\partial^2}{\partial x_i \partial x_k}\left(u_i u_k - \langle u_i u_k \rangle \right) + 2\frac{\partial u_k}{\partial x_i}\frac{\partial U_i}{\partial x_k} \qquad (9)$$

with solution

$$\frac{p(\underline{x})}{\rho} = \frac{1}{4\pi}\int_V \left[\left[\frac{\partial^2}{\partial x_i \partial x_k}(u_i u_k - \langle u_i u_k\rangle) + 2\frac{\partial u_k \partial U_i}{\partial x_i \partial x_k}\right]^{(\underline{x}')} \frac{dV}{|\underline{x}' - \underline{x}|} + \Gamma_{ij} \quad (10)$$

where the integration is carried out over the whole $\underline{x}'$ - space and specified at the point $(\underline{x}')$, and Γ_{ij} is a surface integral. The pressure-strain correlation may be expressed in the form:

$$\frac{p\partial u_i}{\rho \partial x_j} = \frac{1}{4\pi}\int_V \left[\left[\left(\frac{\partial^2 u_l u_m}{\partial x_l \partial x_m}\right)' \frac{\partial u_i}{\partial x_j} + 2\left(\frac{\partial u_m \partial U_l}{\partial x_l \partial x_m}\right)' \frac{\partial u_i}{\partial x_j}\right] \frac{dV}{|\underline{x}' - \underline{x}|} + \Gamma_{ij} \quad (11)$$

this equation shows that the pressure-strain originates from the interaction between turbulence components ($(\phi_{ij})_{,1}$) and from the interaction of the mean rate of strain with turbulence ($(\phi_{ij})_{,2}$) . The surface integral is negligible away from the vecinity of a solid boundary.

Most of the modelling work so far has adopted Rotta's (1951) model for ($(\phi_{ij})_{,1}$)

$$(\phi_{ij})_{,1} = -c_1 \frac{\varepsilon}{k}\left(\langle u_i u_j\rangle - \frac{2}{3}\delta_{ij}\right) \quad (12)$$

where c_1 is a constant, k and ε are the time averaged turbulent kinetic energy and the dissipation energy respectively, the quotient $\frac{k}{\varepsilon}$ thus represents a characteristic decay time of turbulence.

The mean strain contribution to the correlation $\overline{\frac{p\partial u_i}{\rho \partial x_j}}$ is very often modelled starting from the quasi-isotropic model. This was first published Hanjalic and Launder (1972) and by Launder et al (1973). Other derivations following diferents paths have been proposed by Naot, Shavit and Wolfshtein (1972) and Lumley (1973). Launder Reece and Rodi (1975) extended this model to take in account 'wall-echo' effects. Erdogan, Boysan and Swithenbank (1980) assumed a constitutive equation for this term, the pressure-strain being a function of the mean rate of strain tensor $\underline{E}$, the mean rotation tensor $\underline{\Omega}$ and the Reynolds stress tensor $\underline{a}$ and a similar expression to that obtained by the quasi-isotropic model is reached with three independent parameters being made as a function of the local ratio of production to dissipation $\frac{P}{\varepsilon}$. Lin and Wolfhstein (1979) have assumed a complete different approach, arriving at a more complicated form but is work still remains to be tested in more than simple flow situation

3. Non-linear Model for the Pressure-strain term

3.1 The Quasy-Isotropic Non-linear Model

In simulating $(\phi_{ij})_{,1}$ Rotta's proposal can be expanded incorporating non-linear terms as follows:

$$(\phi_{ij})_{,1} = -\frac{\varepsilon}{k}(c_1+c_1' II)(\langle u_i u_j\rangle - \frac{2}{3}\delta_{ij}) - c_1''\frac{\varepsilon}{k^2}(\langle u_i u_k\rangle\langle u_k u_j\rangle - \frac{1}{3}\langle u_r u_s\rangle\langle u_s u_r\rangle\delta_{ij})$$

where c_1 , c_1' and c_1'' are constanst to be adjusted, and II denotes the turbulence anisotropy

$$II = \frac{1}{k^2}(\langle u_i u_j \rangle - \frac{2}{3}\delta_{ij})(\langle u_i u_j \rangle - \frac{2}{3}\delta_{ij}) = b_{ik}b_{kj} \qquad (13)$$

In simulating $(\phi_{ij})_{,2}$ following LRR (1975) it is assumed that this correlation may be aproximated in the form:

$$(\phi_{ij})_{,2} = a^{mi}_{lj}\frac{\partial U_l}{\partial x_m}$$

where

$$a^{mi}_{lj} = -\frac{1}{2\pi}\int_V \frac{\partial^2 u'_m u_i \; dV}{\partial \xi_l \partial \xi_j |\underline{x}' - \underline{x}|} \qquad (14)$$

and the $\xi_{,s}$ are the cartesians components of the position vector $|\underline{x}' - \underline{x}|$. This expression is exact for homogeneous flows but aproximately true in more general flows.

Rotta (1951) has commented that the fourth order tensor a^{mi}_{lj} should satisfy the following kinematic costraints:

(i) $a^{mi}_{lj} = a^{im}_{lj} = a^{mi}_{jl}$ (Symmetry)

(ii) $a^{mk}_{lk} = 0$ (Continuity)

(iii) $a_{kk}^{mi} = 2\langle u_m u_i \rangle$ (Green's Theorem)

The most general expression for this quasy-isotropic model including non-linear terms is:

$$a_{lj}^{mi} = \underset{[1]}{\alpha\langle u_m u_i\rangle\delta_{lj}} + \underset{[2]}{\beta(\langle u_m u_l\rangle\delta_{ij}} + \underset{[3]}{\langle u_m u_j\rangle\delta_{il}} + \underset{[4]}{\langle u_i u_l\rangle\delta_{mj}} + \underset{[5]}{\langle u_i u_j\rangle\delta_{ml}})$$

$$+ \underset{[6]}{c_2\langle u_l u_j\rangle\delta_{mi}} + \underset{[7]}{k(\nu\delta_{mi}\delta_{lj}} + \underset{[8]}{\eta(\delta_{ml}\delta_{ij}} + \underset{[9]}{\delta_{mj}\delta_{il}}))$$

$$+ \underset{[10]}{\alpha'\frac{\langle u_m u_i\rangle}{k}\langle u_l u_j\rangle} + \underset{[11]}{\beta'(\frac{\langle u_m u_l\rangle}{k}\langle u_i u_j\rangle} + \underset{[12]}{\frac{\langle u_m u_j\rangle}{k}\langle u_i u_l\rangle})$$

$$+ \underset{[13]}{\alpha''\frac{\langle u_l u_k\rangle}{k}\langle u_k u_i\rangle\delta_{mj}} + \underset{[14]}{\frac{\beta''}{k}(\langle u_m u_k\rangle\langle u_k u_l\rangle\delta_{ij}} + \underset{[15]}{\langle u_m u_k\rangle\langle u_k u_j\rangle\delta_{il}}$$

$$+ \underset{[16]}{\langle u_i u_k\rangle\langle u_j u_k\rangle\delta_{ml}} + \underset{[17]}{\langle u_i u_k\rangle\langle u_l u_k\rangle\delta_{mj}})$$

$$+ \underset{[18]}{c_2'\frac{\langle u_l u_k\rangle}{k}\langle u_j u_k\rangle\delta_{mi}} + \qquad (15)$$

$$+ \underset{[19]}{\frac{\langle u_p u_q\rangle\langle u_q u_p\rangle}{k^2}(\nu'\delta_{mi}\delta_{lj}} + \underset{[20]}{\eta'(\delta_{ml}\delta_{ij}} + \underset{[21]}{\delta_{mj}\delta_{il}}))k$$

where

α, β, α', β', α'', β'', ν, η, ν', η', c_2, and c_2' are constants.

A linear expression can be obtained by simply putting α', β', ν', η', c_2', α'' and β'' equals to zero and by using the constraints one obtains

$$\alpha\langle u_m u_l\rangle + 5\beta\langle u_m u_l\rangle + c_2\langle u_m u_l\rangle + k\delta_{ml}(2\beta + \nu + 4\eta) = 0 \qquad \text{(ii)}$$

and

$$(3\alpha + 4\beta)\langle u_m u_i\rangle + k(2c_2 + 3\nu + 2\eta)\delta_{mi} = 2\langle u_m u_i\rangle \qquad \text{(iii)}$$

which gives 4 equations in 5 unknowns

$$\left.\begin{aligned} &\alpha + 5\beta + c2 = 0\\ &2\beta + \nu + 4\eta = 0\\ &3\alpha + 4\beta = 0\\ &2c_2 + 3\nu + \eta = 0 \end{aligned}\right] \qquad \text{(16.a)}$$

α, β, ν and η can be determineds in term of c_2 as:

$$\alpha = \frac{1}{11}(4c_2 + 10) \qquad \beta = -\frac{1}{11}(3c_2 + 2)$$

$$\eta = \frac{1}{55}(20c_2 + 2) \qquad \nu = -\frac{1}{55}(50c_2 + 4)$$

In a similar way also the coefficients for the linear + non linear model can be obtained as follows.

$$a^{mk}_{lk} = 0 \qquad \text{(Continuity)}$$

$$(\alpha + 5\beta + c_2 + 2\beta')\langle u_m u_l\rangle + k\delta_{ml}(2\beta + \nu + 4\eta) + \ldots$$

$$+ \frac{\langle u_m u_k\rangle}{k}\langle u_l u_k\rangle(\alpha' + \beta' + \alpha'' + 5\beta'' + c_2') + \frac{(\langle u_p u_q\rangle\langle u_q u_p\rangle)}{k^2} k\delta_{ml}(\beta'' + \nu' + 4\eta') = 0$$

giving

$$\left.\begin{aligned} &\alpha + 5\beta + c_2 + 2\beta' = 0 \\ &2\beta + \nu + 4\eta = 0 \end{aligned}\right] \qquad (16.b)$$

$$\alpha' + \beta' + \alpha'' + 5\beta'' + c_2' = 0$$

$$\beta'' + \nu' + 4\eta' = 0$$

and from the Green's Theorem $a^{mi}_{kk} = 2\langle u_m u_i\rangle$

$$2\langle u_m u_i\rangle = \langle u_m u_i\rangle(3\alpha + 4\beta + 2\alpha') + \delta_{mi}k(2c_2 + 3\nu + 2\eta) + \ldots$$

$$\frac{\langle u_m u_k\rangle}{k}\langle u_k u_i\rangle(2\beta' + 3\alpha'' + 4\beta'') + \frac{\langle u_p u_q\rangle\langle u_q u_q\rangle}{k^2} k\delta_{mi}(c_2' + 3\nu' + 2\eta$$

$$\left.\begin{aligned} &3\alpha + 4\beta + 2\alpha' = 2 \\ &2c_2 + 3\nu + 2\eta = 0 \end{aligned}\right] \qquad (16.c)$$

$$2\beta' + 3\alpha'' + 4\beta'' = 0$$

$$c_2' + 3\nu' + 2\eta' = 0$$

The result is a system of 8 equations with 11 unknowns

Refering to (15) we and collecting terms to get

$$(\phi)_{,2} = \underset{[1]}{-(\alpha + \beta)P_{ij}} \underset{[3]}{- \beta P_{kk}\delta_{ij}} \underset{[2]}{- (c_2 + \beta)D_{ij}} \underset{[6]}{+ (\alpha' + \beta')S_{ij}} \underset{[5]}{+} \underset{[10]}{} \underset{[12]}{} +$$

$$\ldots \underset{[13]}{+ (\alpha'' + \beta'')T_{ij}} \underset{[15]}{+ (\beta'' + c_2)V_{ij}} \underset{[17]}{} \underset{[18]}{} \underset{[11]}{- \beta' P_{kk}\frac{\langle u_i u_j \rangle}{k}} +$$

$$\ldots + k\left[\underset{[7]}{(\nu + \eta)} \underset{[9]}{} + \underset{[19]}{(\nu' + \eta')} \underset{[21]}{\frac{\langle u_p u_q \rangle \langle u_q u_p \rangle}{k^2}}\right] E_{ij} + \underset{[14]}{\beta'' S_{kk}\delta_{ij}}$$

numbers in square brackets underneath the terms refer to those in equation (15); with E_{ij}, P_{ij}, and D_{ij} having the following meaning:

$$E_{ij} = \frac{\partial U_i}{\partial x_j} + \frac{\partial U_j}{\partial x_i}$$

$$P_{ij} = -(\langle u_i u_k \rangle \frac{\partial U_j}{\partial x_k} + \langle u_j u_k \rangle \frac{\partial U_i}{\partial x_k})$$

$$D_{ij} = -(\langle u_i u_k \rangle \frac{\partial U_k}{\partial x_j} + \langle u_j u_k \rangle \frac{\partial U_k}{\partial x_i})$$

also S_{ij}, T_{ij} and V_{ij} are the following tensors

$$S_{ij} = \frac{1}{k}(\langle u_m u_i \rangle \langle u_l u_j \rangle + \langle u_m u_j \rangle \langle u_l u_i \rangle) \frac{\partial U_i}{\partial x_m}$$

$$T_{ij} = \frac{1}{k}(\langle u_k u_i \rangle \langle u_m u_k \rangle \frac{\partial U_j}{\partial x_m} + \langle u_k u_j \rangle \langle u_m u_k \rangle \frac{\partial U_i}{\partial x_m})$$

$$V_{ij} = \frac{1}{k}(\langle u_i u_k \rangle \langle u_l u_k \rangle \frac{\partial U_l}{\partial x_j} + \langle u_j u_k \rangle \langle u_l u_k \rangle \frac{\partial U_l}{\partial x_i})$$

and $S_{kk} = T_{kk} = V_{kk}$

It can be noted that due to continuity in an incompressible fluid the constribution of the terms [4], [8], [16] and [20] is zero; the term [11] is incorporated into $(\phi_{ij})_{,1}$ and neglected since its variation is similar to that of the second invariant. Collecting all terms we obtain the final form of this non-linear model.

$$\phi_{ij} = (\phi_{ij})_{,1} + A_1(P_{ij} - \frac{1}{3}P_{kk}\delta_{ij}) + (A_2 + A_2' \frac{\langle u_p u_q \rangle \langle u_q u_p \rangle}{k^2}) kE_{ij}$$

$$+ A_3(D_{ij} - \frac{1}{3}D_{kk}\delta_{ij}) + A_4(S_{ij} - \frac{1}{3}S_{kk}\delta_{ij})$$

$$+ A_5(T_{ij}-\frac{1}{3}T_{kk}\delta_{ij}) + A_6(V_{ij}-\frac{1}{3}V_{kk}\delta_{ij}) \qquad (16)$$

where

$$A_1 = -(\alpha+\beta) \qquad A_2 = (\nu+\eta) \qquad A_2' = (\nu'+\eta')$$

$$A_3 = -(c_2+\beta) \qquad A_4 = (\alpha'+\beta') \qquad A_5 = (\alpha''+\beta'')$$

$$A_6 = (\beta''+c_2')$$

By comparing equations (16.b) and (16.c) with equation (16.a) from the linear case it can be noted that only the constants α' and β' are absent from (16.a). It may be concluded, although not definetely, that α' and β' are the principal non-linear constributions to a_{1j}^{mi} and so we can neglect α'' , β'' , η' and ν'. Now expressing α, β, η, and ν in terms of c_2, α' and β' ie.:

$$\alpha = \frac{1}{11}(4c_2+10(1-\alpha')+8\beta') \qquad \beta = -\frac{1}{11}(3c_2+2(1-\alpha')+6\beta')$$

$$\eta = \frac{1}{55}(20c_2+(1-\alpha')+18\beta') \qquad \nu = -\frac{1}{55}(50c_2+4(1-\alpha')+12\beta')$$

therefore the coefficients A_1 , A_2 , A_3 and A_4 of equation (16) become

$$A_1 = -\frac{1}{11}(c_2+8(1-\alpha')+2\beta') \qquad A_2 = -\frac{1}{55}(30c_2-2(1-\alpha')-6\beta')$$

$$A_3 = -\frac{1}{11}(8c_2-2(1-\alpha')-6\beta') \qquad A_4 = (\alpha'+\beta')$$

for $\alpha' = \beta' = 0$, A_1 , A_2 , A_3 and A_4 reduces to the linear quasi-isotropic model of LRR.

Equation (16) is the most general form of the pressure-strain correlation and an optimization for all the constants is a difficult task, it may be then be reasonable to look for a simplified version. In the next section a new approach is considered in which it is assumed that the parameter c_2 of the standard LRR Model is sensitive to the anisotropy of the flow.

3.2 Pressure-strain Model with c_2 as a function of the invariants

In our investigation we have found that in solving the differential equations for Harris et al. flow using LRR model, a constant value for c_2 fail to predict the level of tne shear stress $\overline{uv}$ and consequently giving unsatisfactory predictions for the other Reynolds stresses; similarly in the turbulence undergoing axisymmetric strain the linear and non-linear quasi-isotropic model are unable to reproduce the deflection of energy to the longitudinal component. It is possible to improve this situation without affecting the predictions for the other flow considered, by assuming that c_2 is influenced by the state of anisotopy of the flow and so c_2 is taken as a function of the second and third invariant of the anisotropy tensor, ie:

$$c_2 = 0.4 + a_1 b_{ik} b_{kj} + a_2 b_{ik} b_{kj} b_{ji}$$

where

$$b_{ij} = \frac{\langle u_i u_j \rangle}{k} - \frac{2}{3}\delta_{ij} \quad , a_1 \text{ and } a_2 \text{ are constants,}$$

although so far only the second invariant has been taken into account.

4. Homogeneous Turbulent Flows

Homogeneous turbulent flows are physical models on which the turbulent motion is simpler, they can be described by coupled ordinary differential equations. Theses flow configurations are the "ideal" cases for computational modelling. Flow of this class may be devided in three groups

(i) Homogeneous isotropic turbulence. This is the simplest type of turbulence. In spite of the fact that it is unrealistic a knowledge of its structure and behaviour has provided the basis for a better understanding of non-isotropic flows.

(ii) A second physical model is the homogeneous non-isotropic turbulence with no mean velocity gradients. In this situation there is a strong tendency towards isotropy and so the first part of the pressure-strain plays a significant role. For this and the above group the turbulent kinetic energy is always decaying since there is only redistribution and dissipation of energy (we have used the experimental data of Uberoi (1956) and Tuckers and

Reynolds (1968)).

(ii) A third physical model is the homogeneous non-isotropic turbulence with constant mean velocity gradient. In this configuration there is producction, redistribution and dissipation of energy. We may subdivide this group in flows of two kind:

Uniform pure strain : In this case the principal axes of the Reynolds stresses are the same as those of the mean rate of strain. We have considered:

Plane strain (Townsend (1956), Tucker and Reynolds (1968)).

Axisymetric contraction (Uberoi (1956) Tan-atichat (1980)).

Uniform rotational strain : In this case the axes of the Reynolds stresses are not aligned with the axes of the mean rate of strain. We have taken for this kind of flow the experiments of Champagne et al (1970) and Harris et al. (1977).

Table I summarizes the flows with their initial conditions which we have been used in the numerical computation.

5. Numerical Computation

Solving the Differential Equations. The description of these turbulent flows was done by solving the coupled differential equations for the Reynolds stresses with their initial conditions and the dissipation equation :

$$\frac{\partial \langle u_i u_j \rangle}{\partial t} = P_{ij} + (\phi_{ij})_{,1} + (\phi_{ij})_{,2} - \frac{2}{3}\varepsilon$$

$$\frac{\partial \varepsilon}{\partial t} = \frac{\varepsilon}{k}(c_{\varepsilon 1} P - c_{\varepsilon 2}\varepsilon)$$

where

$$\frac{\partial}{\partial t} = U\frac{\partial}{\partial x} \quad , \text{ and} \quad c_{\varepsilon 1} = 1.44 \quad , \quad c_{\varepsilon 2} = 1.92$$

Programs employing Euler-First order method were used except for the axisymetric contraction where a variable-order, variable-step Adams method (1976) was used. The presssure-strain models were incorporated in these programs and the constants were adjusted to obtain satisfactory good results for all the flow situation. Table 2 shows the constants for all the models; Model I refers to the full non-linear expression, Model II(1) and Model II(2) refer to the the expression with c_2 as a function of the second and second + third invariant respectively.

6. Results and Discussion

6.1 Return to Isotropy

Figures F-01 and F-02 shows the comparison between Uberoi (1956) experiments and the predictions for the Model I and Model LRR (in this case Model II reduces to LRR); it seems that a best perfomance is obtained when the first part of the pressure-strain is expressed in a non-linear form. However not much improvement is gained for the plane flow plotted in F-03.

6.2 Uniform Plane-strain

Figures F-04 shows the computed and measured behaviour of the flow studied by Townsend. Not a great difference is obseved in the predictions of the three models although Model II(1) shows better agreement with the experiments. Turning to Tucker and Reynolds experiment figure F-05 shows the perfomance of these models; it appears that all models fail to predict the rise of the v^2 component at the end of the contraction and in particular the non-linear model whose rate of transfer of energy among components seems to be small.

6.3 Axisymmetric Contraction

Figures F-06, F-07, F-08 show the computed and measured results for three cases taken from Tan-atichat experiments for which the strain rate is no constant. In all cases studied the models were unable to reproduce the sudden increase of the streamwise component arising from the acceleration. For the LRR model this is consistent with the behaviour described by Launder

Reece and Rodi (1975) when observing Uberoi's (1956) 16:1 axisymmetric experiment. For the non-linear model the effect is quite the contrary, the transverse component is overpredicted and the rate of transfer of energy is small; the reason for this behaviour seems to be the introduction of the new term S_{ij} with a negative value for the respective constant and so it makes a negative constribution to u^2 and a positive to v^2, therefore it does not tend to change the trend of both components. The same situation is reproduced for Uberoi's experiments plotted in figures F-08 and F-09. Figure F- 13 shows experimental results and predictions using Model I and Model II(2) for Tan-atichat experiments, it seems that the introduction of the third invariant has a favourable effect.

6.4 Shear turbulence

Turning to Champagne et al. experiment it can be seen in figures F-11 that the models reproduce almost the same behaviour but Model I (non-linear) is inferior since underpredict the shear component. Besides the level of turbulence energy at the end of the computation is underpredicted for all models.

Finally figures F-12 show the shear flow of Harris et al. , here the three models behave very different. The u^2 and the v^2 components are overpredicted by LRR Model , Model I (non-linear) gives better agreement but model II (c_2 variable) seems to be the best. Predictions for v^2 are unsatisfactory for all

models. The shear stress level is again overpredicted by LRR model and this seems to be the reason why the predictions for the other components are unsatisfactory. An overall better agreement is obtained with Model I and II(1) and in particular in figure F-14 a satisfactory improvement is obseved when using model II(2).

7. Concluding Remarks

A general expression for the pressure-strain term of the Reynolds stress equation have been studied and applied to a number of turbulent hommogeneous flows. Considering possible errors arising from the strongly coupled non-linear differential equations and the difficulties in optimising simultaneously the constants involved the overall predictions are satifactory. The simpler version which contains the invariants seems to be the appropriate way for further improvements, this idea should be extended to the simpler model of Gibson and Launder (1976) and look into the effects of varying the "constant" associated with the anisotropy of the production.

8. References

Champagne, F. H., Harris, V.G. & Corrsin, S. (1970) "Experiments on nearly homogeneous turbulent shear flow". J. Fluid Mech. 41, 81-139.

Chou, P. Y. (1945) "On velocity correlations and the solution of the equations of turbulence fluctuation". Quart. Appl. Math. , 3, 38-54.

Daly, B. J. & Harlow, F. H. (1970) "Transport equations of turbulence", Phys. Fluids, 13, 2634-2649

Erdogan, M. E., Boysan, F. and Swithenbank, J. "On the Prediction of Reynolds stresses". Internal Report, Depto of Chemical Engineering and Fuel Tech., Sheffield University

Ferziger, J. H. (1980). "Homogeneous turbulent flows: a review and evaluation", Report for the 1980-81 AFOSR-HTTM-Standford Conference on Complex Turbulent Flows.

Gibson, M.M. and Launder, B. E. (1976) "On the calculations of horizontal free shear flows under gravitational influence". ASME J. Heat Transfer, 98C, 80

Hall, G. , and Watt, J. M. "Moderns Numerical Methods for Ordinary Differential Equations". Clarendom Press, Oxford 1976

Hanjalic, K. & Launder, B. E. "A Reynolds stress model of turbulence and its application to thin shear layer flows". J. Fluids Mech. 52, 609-638.

Harris, V. G., Graham, J. A. H. & Corrsin, S. (1977) " Further experiments on nearly homogeneous shear flow". J. Fluid Mech. 81, 657-687.

Launder, B. E., Reece, G. J. & Rodi, W. (1975) " Progress in the development of a Reynolds stress turbulence closure". J. Fluids Mech., 68, 537-566.

Launder, B. E., Morse, A. P., Rodi, W., and Spalding, D. B., "The prediction of Free Shear Flows- A Comparison of the Perfomance of Six Turbulence Models", Proceedings of the Langley Free Shear Flows Conference, NASA SP321, Vol.1 (1973).

Lin, A. & Wolfshtein, M. "Theoretical Study of the Reynolds stress equation"., Turbulent Shear Flows I (1979), 327-343

Lumley, J. L., "Prediction Methods for Turbulent Flows- Introduction", Lectures Series 76 (Von Karman Institute 1975).

Naot, D., Shavit, a., and Wholfshtein, M., "Two point correlation model and the redistribution of Reynolds stresses", Phys. Fluids 16, 6 (1973)

Rodi, W. (1976) "A new algebraic relation for calculating the Reynolds stress. ZAMM, 56, T219-t221.

Rotta. J. C. (1951) "Statistische Theorie nichthomogener Turbulenz. Z. Phys., 129, 547-572.

Tan-atichat, J. (1980) "Effects of axisymmetric contractions on turbulence of various scales" Ph.D. Thesis, Illinois Institute of Technology.

Townsend, A. A. (1956). "The uniform distortion of homogeneous turbulence", Q. J. Mech. Applied Math., 7, 104.

Tucker, H. J. , & A. J. Reynolds (1968). " The distortion of turbulence by irrotational plane strain", J. Fluid Mech., 32, 657

Uberoi, M. S. (1956). "Effect of wind tunnel contraction on free stream turbulence", J. Aero. Sci. 754. .

Report on the Modelling and Measurements made on a Dump Combustor

As detailed in the introduction, part of the effort of the past year has been to investigate various flow fields associated with an axial entry type dump combustor.

During the past year a dump combustor has been built and is shown below. This is suitable for hot and cold flows and has optical access at its inlet and along its 1 metre length. The inlet and dump sections have 80 mm and 160 mm diameters respectively and with the air facility available, inlet velocities of 100 M/s are possible.

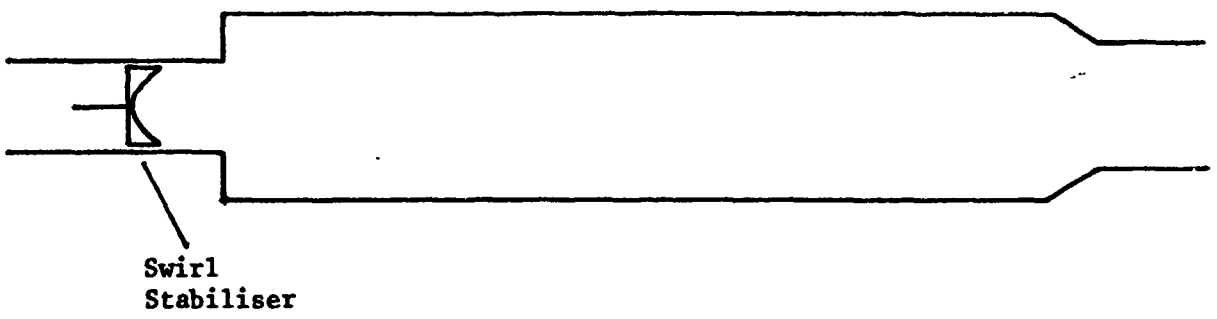

Dump combustor geometry used in the measurement study. The inlet section is segmented allowing replacement of the swirl stabiliser by a baffle at the same position or at the dump plane.

Calculations and Measurements

The work to be described concerns measurements and calculations for the following inlet conditions a) no stabiliser b) a three element baffle at the dump plane c) a three element baffle at 8 cm upstream of the dump plane d) a swirl stabiliser at 8 cm upstream of the dump plane.

In all cases k - ε modelling of the flow field has been applied and in the swirl case, different levels of the algebraic model have been used. In addition for the baffle case, combustion calculations have been performed.

The baffle used consisted of thin plate with rectangular obstructions of 30% total blockage area. For the swirler the design was based on the work of Buckley et al at AFWAL and employed computed blade shapes. Results for an approximate free vortex swirler of swirl number 0.4 are reported here.

The LDA system employed consisted of a backscatter arrangement with frequency shifting, and signal processing was by means of a burst correlator. The light from a 488 nm argon laser was focused onto a rotating diffraction grating using a 200 mm lens. This ensures a circular cross section of the diffracted beams thus maximising subsequent beam crossing and minimising uncorrelated noise. Two furhter lenses collimate the $\pm$ orders and also permit the choice of beam separation and hence fringe spacing.

The beams are focused and crossed by means of an output lens of 1500 mm focal length thus providing some considerable distance between the test rig and the instrumentation. For single photon collection, as with this configuration, data processing is by autocorrelation and summation, resulting in accumulated autocorrelation functions containing all velocity variations occurring during the sampling interval.

Each sampling operation is controlled by a PET microcomputer and data is analysed by a curve fitting procedure.

The collection system, which was aligned at 15° to the output axis as a means of obtaining the desired the longitudinal resolution, consisted of a 750 mm focal length collection lens of 112 mm aperture focusing onto a collection pinhole which controlled the lateral resolution.

A Malvern Instruments RF313 photmultiplier, which was capable of observing single photons, was focused on the collection pinhole and fed its output to the 50 nsec correlator.

In a typical experimental run the test rig, which is on a motor driven traverse, is scanned across the region of interest, with the fringe velocity being measured at each sample point simultaneously by feeding the counting pulses from a grating monitor to one of the correlator storage channels.

For the present work, the fringe velocity employed was up to 130 M/s depending on the turbulence level, and the fringe spacing was 88 μ. The spatial resolution, which is determined largely by the angle of collection and waist diameter at the probe volume, was around 1 mm both longitudinally and laterally, based on a 100 times drop in collected signal strength at these limits. The air velocities used at the 80 mm diameter inlet were between 65 and 75 M/S being limited by the supply, and seeding was by means of 0.5 μ source particles of titanium dioxide generated in a 10 cm diameter and 120 cm high fluidised bed.

Background noise limited the closest approach to the walls to 9.24 mm.

Results

Isothermal Flows

The first results are shown in Figure 15 and show a comparison of calculated and measured velocities at three axial stations. For each profile two cases are displayed - with the three element at the dump plane and with no baffle stabiliser. For the baffle case, the plane of measurement was on a reflection symmetry plane at 90° from the mid-line of one of the baffles. Also included in the Figure is a comparison of the turbulence levels at one of the stations. In all cases the no baffle condition shows good agreement between measured and calculated velocity and turbulence, showing that in this case, as would be expected, the $k - \varepsilon$ model is satisfactory.

For the case with baffles at the dump plane, the agreement is moderately good at 50 mm from the dump plane but deteriorates as one goes down stream, with the measured values flattening out much more quickly. Examination of the turbulence values indicates that the model has greatly underestimated these, and most likely accounts for the much slower levelling out of the velocity.

Comparisons for the swirl stabilised case are shown in Figure 16 and show calculations based on the $k - \varepsilon$ turbulence model and the algebraic model. It can be seen that both models fall quite far short of representing the flow field accurately. However for the algebraic model, there is a small region of reverse flow on the axis as found experimentally. This was a difficult feature to reproduce and only resulted when a full solution of the stress transport equations was applied.

These results contrast strongly with the simpler swirling case associated with tangential entry devices, which the algebraic model has represented very well and indicates that for flows with swirl introduced at the axis, further development work is required.

To investigate the models further, measurements and calculations using the k - ε model have been carried out on the same geometry with the baffles situated at 8 cm upstream of the dump plane.
Experimentally, this results in the same turbulence levels but a greatly reduced recirculation bubble at the dump plane. Figure 17 shows the comparison results at the 150 mm position . It can be seen here that the agreement is much better than with the baffle at the dump plane indicating that the strong recirculation in the first case is reducing the closeness of fit of the k - ε calculated fields.

Combustion Case

Figures 18,19and 20 show some typical results which can be obtained for fuel spray combustion. The three element baffle has been used here and a single spray is injected from upstream at right angles to the wall.
A distribution of drop sizes is employed ranging from 5 μ to 100 μ, with a Rosin Rammler distribution of mean 50 μ and width parameter of 2.2.
Preheated air at 550°K is used as input and a fuel air ratio of 0.02 is used. Figure 18 shows the trajectory and evaporation history of ten drops of different size. The smallest penetrate least into the flow and are convested inside the dump. The croses show the points at which they evaporate. It can also be seen that some of the larger droplets do not evaporate within the range considered and it is clear that this kind of study is of some value in matching a particular atomiser to the flow field.
Figure 19 is derived from the information of the kind seen in Figure for each computational cell and shows a contour of constant evaporated fuel mass fraction. This is invaluable information in indicating where unburnt evaporated fuel originates and is convected. It can be seen from the figure that the pattern is following the general flow field and then becoming entrained in the strong recirculation zone behind the baffles.
Figure 20 is a similar contour plot for temperature at 2000°K and again shows the curvature associated with one of the recirculation bubbles. Such information is useful in association with evaporation patterns in correcting for hot wall regions.

Conclusions

Some of the main features of the flow/combustion model have been described, and the ease of setting up a device geometry has been emphasised.
The dump combustor study has underlined some of the limits of applicability of the k - ε model and, in addition to the axially symmetric swirling flow

these appear also to include flows with strong recirculating zones. From previous work, it appears that a more fundamental approach to the shear stress modelling may correct most of the difficulty in these cases and the incorporation of these new developments for the strongly 3-D case is currently underway.

For the case of swirl introduced around the axial region it was seen that the algebraic stress model of turbulence was able to some degree reproduce the reverse flow on axis, but that there is still considerable room for improvement in this mathematically more difficult case.

Publications (in the last three years)

1. F.Boysan and J.Swithenbank 'Spray Evaporation in Recirculating Flow', 17th Symposium (International) on Combustion, Leeds, 1978
2. F.Boysan 'Spray-Air Interaction With and Without Evaporation', 2nd Intl. Symp. on Multi Phase Flow and Heat Transfer, Miami, 1979
3. F.Boysan and H.Binark 'Predictions of Induced Air Flows in Hollow Cone Sprays', ASME J. Fluids Eng., Sept. 1979
4. F.Boysan, J.Swithenbank 'Prediction of confined Turbulent Vortex Flows', paper presented at ASME Vortex Flows Symp., Chicago, 1980
5. W.H.Ayers, F.Boysan, J.Swithenbank 'Droplet Trajectories in Three Dimensional Gas Turbine Flow Fields', Department of Chemical Eng. and Fuel Technology Report No. HIC 355, 1980
6. F.Boysan, W.H.Ayers,J.Swithenbank, Z.Pan 'Three dimensional Model of Spray Combustion in Gas Turbine Combustors', AIAA J. Energy,6, 6 1982
7. F.Boysan, E.Erdogan, B.C.R.Ewan, J.Swithenbank 'Prediction of Strongly Swirling Turbulent Flows with an Algebraic Reynolds Stress Closure', Department of Chemical Engineering and Fuel technology, Report No. HIC 365, 1981
8. F.Boysan, J.Swithenbank 'Numerical Prediction of Confined Vortex Flows' International Conference on Numerical Methods in Laminar and Turbulent Flows, Venice, Italy, 1981
9. M.E.Erdogan, F.Boysan, J.Swithenbank 'On the calculation of Reynolds Stresses', Department of Chemical Engineering and Fuel Technology, Report No. 347, 1981
10. W.H.Ayers, F.Boysan, J.Swithenbank 'Three dimensional Droplet Trajectories in Gas Turbine Combustors', 5th International Symp. on Air Breathing Engines, Bangalore, India, 1981
11. F.Boysan, W.H.Ayers, J.Swithenbank'A fundamental Mathematical Modelling Approach to Cyclone Design', Transactions I. Chem. E. Vol. 60, 1982
12. F.Boysan, B.C.R.Ewan, J.Swithenbank, W.H.Ayers, 'Experimental and Theoretical Studies of Cyclone Separator Aerodynamics', I. Chem. E. Symposium Series No. 69
13. F.Boysan, R.Weber, J.Swithenbank 'Mathematical Modelling of an Entrained Coal Gasifier', 1983 International Gas Research Conf., London
14. W.H.Ayers, F.Boysan, J.Swithenbank' Fundamental Studies of Two Phase Turbulent Flows in Cyclone Separators', I. Chem. E. Jubilee Symposium London, 1982

Publications (cont'd)

15. W.H.Ayers, F.Boysan, J.Swithenbank, B.C.R.Ewan 'Theoretical Modelling of Cyclone Performance', FILTECH Conference, London, Sept., 1983
16. W.H.Ayers, F.Boysan, B.C.R.Ewan, J.Swithenbank 'Problem Independent Numerical Simulation of Two Phase Flow in Combustors', 62nd Symposium AGARD Propulsion and Energetics Panel, Turkey, Oct., 1983
17. J.Swithenbank, B.C.R.Ewan, W.H.Ayers, F.Boysan 'The prediction and Measurement of Turbulent Mixing in a Gas Turbine Flow', to be published at 20th International Symposium on Combustion, Michigan, Aug., 1984
18. R.Weber, F.Boysan, W.H.Ayers, J.Swithenbank 'Simulation of Dispersion of Heavy Particles in Confined Turbulent Flows', to be published in A.I.Chem.E. J.

TURBULENCE MODELLING

ESTIMATING $\overline{u_i u_j}$

EFFECTIVE VISCOSITY MODELS

$$\nu = C \frac{k^2}{\varepsilon}$$

TRANSPORT EQUATIONS FOR k and ε

BOUSSINESQ HYPOTHESIS

$$\overline{u_i u_j} = \frac{2}{3} k \delta_{ij} - \nu \left(\frac{\delta u_i}{\delta x_j} + \frac{\delta u_j}{\delta x_i} \right)$$

RICHARDSON NUMBER CORRECTION

REDUCE ν FOR u_θ CORRELATIONS

FUNDAMENTAL MODELS

STRESS TRANSPORT EQUATIONS

$$T_{ij} = P_{ij} - \frac{2}{3} \varepsilon \delta_{ij} + \Psi_{ij}$$

ALGEBRAIC MODELS

RODI APPROXIMATION

$$T_{ij} = \frac{\overline{u_i u_j}}{k} (P - \varepsilon)$$

SOLUTION OF DIFFERENTIAL EQUATIONS

P_{ij} = production rate

ε = dissipation rate

Ψ_{ij} = pressure strain ter

FIGURE 1. OPTIONS AVAILABLE FOR TURBULENCE MODELLING.

```
 (*)-     VIEW CELLS
 J   I= 1 2 3 4 5 6 7 8 9101112131415161718192021222324252627282930
 14    WOWOWOWOWOWOWOWOWOWOWOWOWOWOWOWOWOWOWOWOWOWOWOWOWOWOWOWOWO
 13    WOWOWOWOWOWOWOWOWOWO. . . . . . . . . . . . . . . . . . . . 0
 12    WOWOWOWOWOWOWOWOWOWO. . . . . . . . . . . . . . . . . . . . 0
 11    WOWOWOWOWOWOWOWOWOWO. . . . . . . . . . . . . . . . . . . . 0
 10    WOWOWOWOWOWOWOWOWOWO. . . . . . . . . . . . . . . . . . . . 0
  9    WOWOWOWOWOWOWOWOWOWO. . . . . . . . . . . . . . . . . . . . 0
  8    WOWOWOWOWOWOWOWOWOWO. . . . . . . . . . . . . . . . . . . . 0
  7    IO. . . . . . . . . . . . . . . . . . . . . . . . . . . . . 0
  6    IO. . . . . . . . . . . . . . . . . . . . . . . . . . . . . 0
  5    IO. . . . . . . . . . . . . . . . . . . . . . . . . . . . . 0
  4    IO. . . . . . . . . . . . . . . . . . . . . . . . . . . . . 0
  3    IO. . . . . . . . . . . . . . . . . . . . . . . . . . . . . 0
  2    IO. . . . . . . . . . . . . . . . . . . . . . . . . . . . . 0
  1    WOWOWOWOWOWOWOWOWOWOWOWOWOWOWOWOWOWOWOWOWOWOWOWOWOWOWOWOWO

 (SETUP1)-  HE,QU,DD,GA,GE,PC,SC,VC,BC,LB,
SC
 (*)-     *SET CELLS*
 (I)-    ENTER 1ST I
 (I)-      ++(DEFAULT     1)++
9
 (I)-    ENTER 2ND I
 (I)-      ++(DEFAULT    30)++
10
 (I)-    ENTER 1ST J
 (I)-      ++(DEFAULT     1)++
5
 (I)-    ENTER 2ND J
 (I)-      ++(DEFAULT    14)++
7
 (BOUNDS)-  HE,QU,W ,S ,. ,C ,O ,I ,
W
 (I)-    SELECT ZONE
 (I)-      ++(DEFAULT     0)++
0
 (SETUP1)-  HE,QU,DD,GA,GE,PC,SC,VC,BC,LB,
VC
 (*)-     VIEW CELLS
 J   I= 1 2 3 4 5 6 7 8 9101112131415161718192021222324252627282930
 14    WOWOWOWOWOWOWOWOWOWOWOWOWOWOWOWOWOWOWOWOWOWOWOWOWOWOWOWOWO
 13    WOWOWOWOWOWOWOWOWOWO. . . . . . . . . . . . . . . . . . . . 0
 12    WOWOWOWOWOWOWOWOWOWO. . . . . . . . . . . . . . . . . . . . 0
 11    WOWOWOWOWOWOWOWOWOWO. . . . . . . . . . . . . . . . . . . . 0
 10    WOWOWOWOWOWOWOWOWOWO. . . . . . . . . . . . . . . . . . . . 0
  9    WOWOWOWOWOWOWOWOWOWO. . . . . . . . . . . . . . . . . . . . 0
  8    WOWOWOWOWOWOWOWOWOWO. . . . . . . . . . . . . . . . . . . . 0
  7    IO. . . . . . . WOWO. . . . . . . . . . . . . . . . . . . . 0
  6    IO. . . . . . . WOWO. . . . . . . . . . . . . . . . . . . . 0
  5    IO. . . . . . . WOWO. . . . . . . . . . . . . . . . . . . . 0
  4    IO. . . . . . . . . . . . . . . . . . . . . . . . . . . . . 0
  3    IO. . . . . . . . . . . . . . . . . . . . . . . . . . . . . 0
  2    IO. . . . . . . . . . . . . . . . . . . . . . . . . . . . . 0
  1    WOWOWOWOWOWOWOWOWOWOWOWOWOWOWOWOWOWOWOWOWOWOWOWOWOWOWOWOWO

 (SETUP1)-  HE,QU,DD,GA,GE,PC,SC,VC,BC,LB,
```

FIGURE 2 Demonstration of system geometry specification within combustion/flow algorithm. This part of the print out shows the introduction of a baffle at the exit of a dump combustor. W = Wall, I = Inlet.

TABLE I

Case Title	Fig. No.	Other Data	Initial Conditions (t or x = 0) u^2	v^2	w^2	ε
Return to isotropy						
Uberoi	F-01	CR=4, Re=3710	1.99×10^{-4}	1.54×10^{-4}	1.54×10^{-3}	3.62×10^{-3}
	F-02	CR=4, Re=12300	3.12×10^{-3}	2.43×10^{-2}	2.43×10^{-2}	17.11×10^{-2}
Tucker & Reynolds	F-03		1.29×10^{-2}	1.79×10^{-2}	4.2×10^{-3}	1.89×10^{-3}
Uniform Strain						
Irotational (i)						
Plane Strain						
Townsend	F-04	SR= 9.44	2.44×10^{-2}	2.66×10^{-2}	2.20×10^{-2}	59
Tucker & Reynolds	F-05	SR= 4.45	4.02×10^{-2}	3.07×10^{-2}	2.68×10^{-2}	0.63
Axisymetric strain						
Tan-atichat (1)	F-06		3.53×10^{-3}	2.46×10^{-3}	2.46×10^{-3}	0.039
	F-07		2.58×10^{-3}	2.16×10^{-3}	2.16×10^{-3}	0.024
	F-08		1.90×10^{-3}	1.72×10^{-3}	1.72×10^{-3}	0.016
Uberoi	F-09		0.016	0.013	0.013	0.040
	F-10		0.015	0.09	0.09	0.044
Rotational (ii)						
Champagne et al.	F-11	SR=12.9 (*)	6.29×10^{-2}	5.51×10^{-2}	4.98×10^{-2}	0.935
Harris et al.	F-12	SR=48.0 (**)	1.87×10^{-1}	7.50×10^{-2}	9.32×10^{-2}	1.61

SR is the strain rate
(*) uv(0)=-0.0154, (**) uv(0)=-0.0574
units for variables are metres and seconds
(1) Rate of strain variable, taken from Ferziger (1980)

TABLE 2

Constants	LRR	Model I	Model II(1)	Model II(2)
c_1	1.5	1.9	1.5	1.5
c'_1	-	-1.1	-	-
c''_1	-	0.21	-	-
c_2	0.4	0.48	0.4+0.45II	0.4+0.27II+1.9III
α'	-	0.0	-	-
β'	-	-0.14	-	-

II and III are the second and third invariant of the anisotropy tensor given by:

$$II = b_{ik}b_{ki} \quad \text{and} \quad II = b_{ik}b_{kj}b_{ji}$$

MODEL LRR

MODEL 4

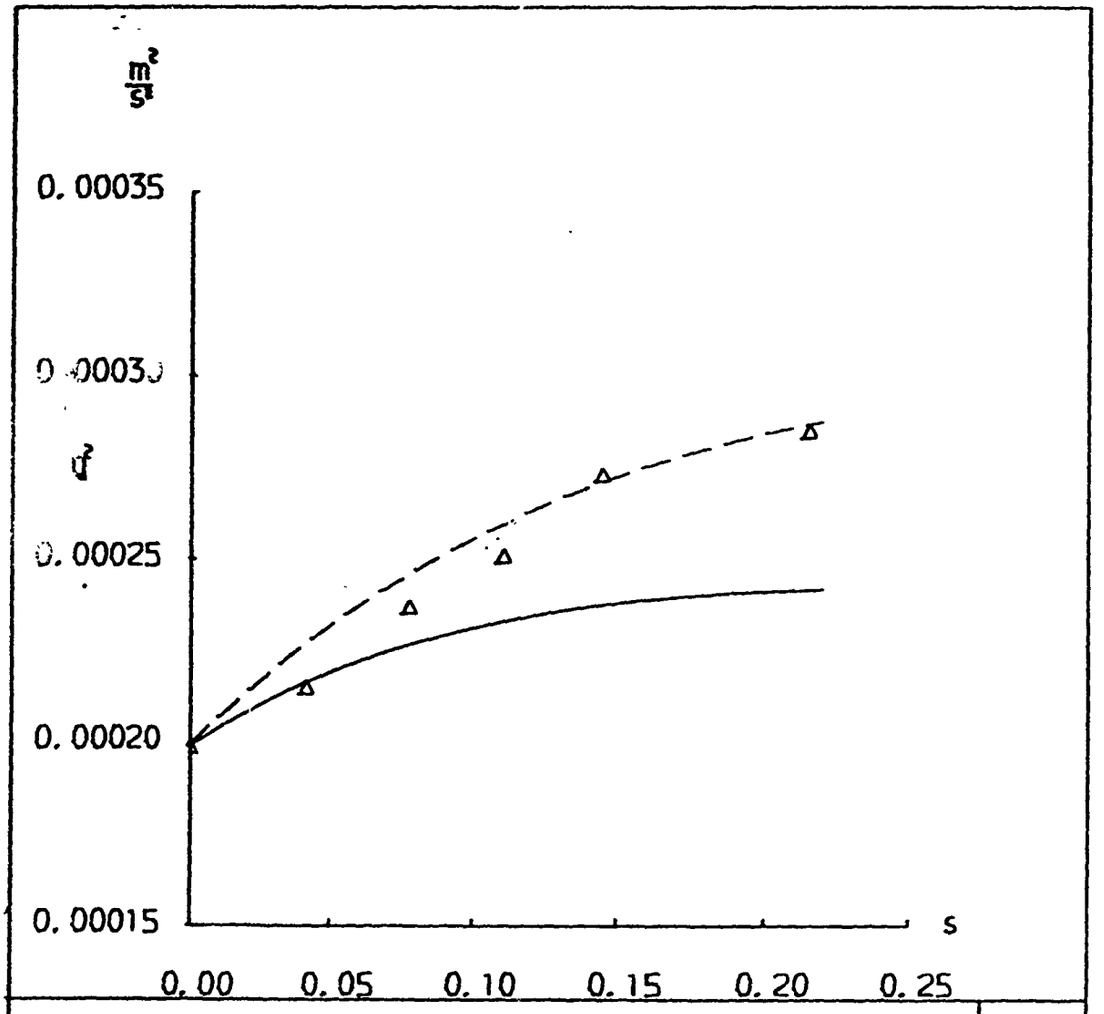

AXISYMETRIC RETURN TO ISOTROPY. UBEROI

U-FLUCT. VELOCITY / ELAPSED TIME

F-01

——— MODEL LRR

- - - - MODEL-I

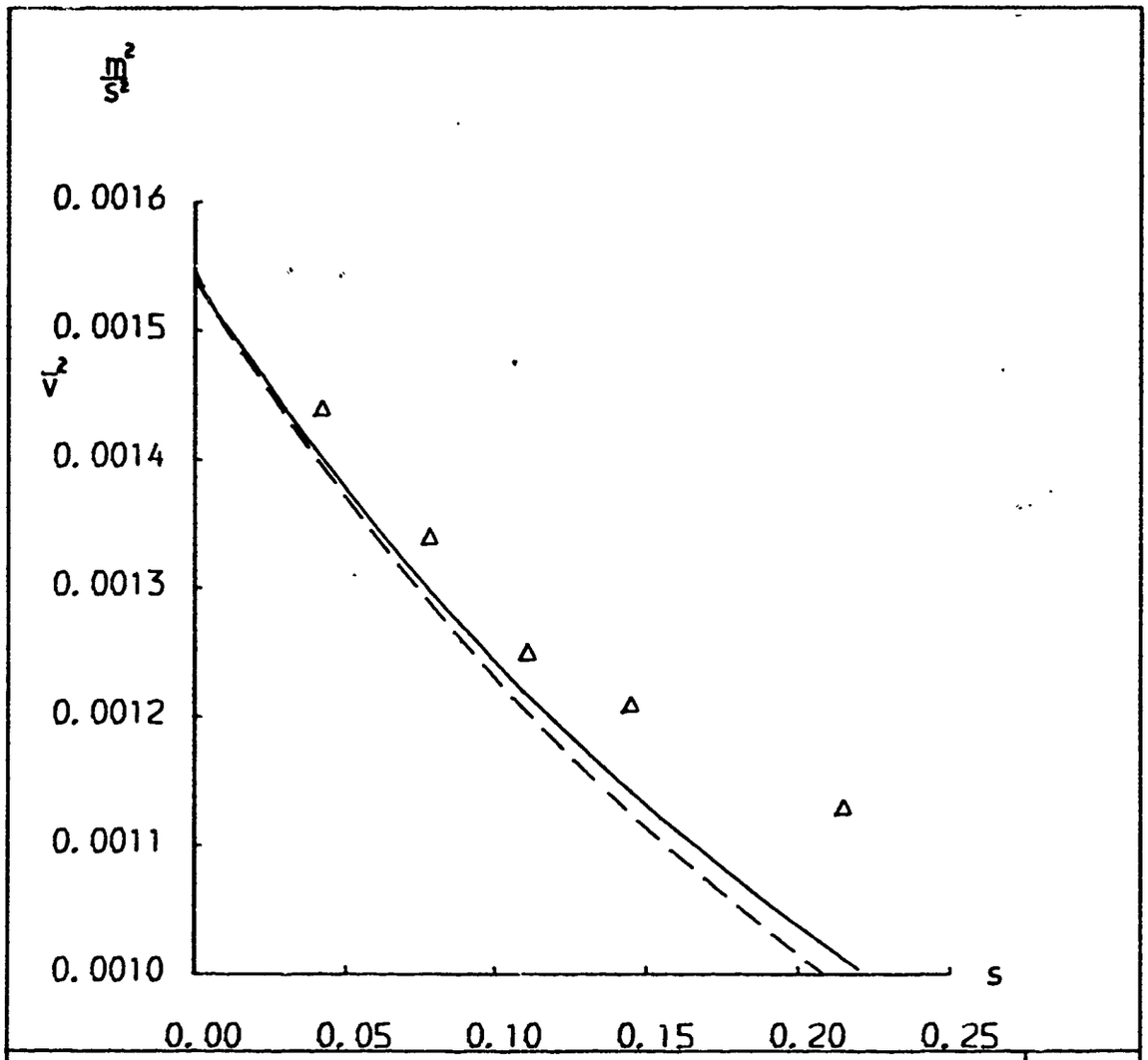

AXISYMETRIC RETURN TO ISOTROPY: UBEROI

V-FLUCT. VELOCITY / ELAPSED TIME

F-01

—— MODEL LRR

- - - - MODEL I

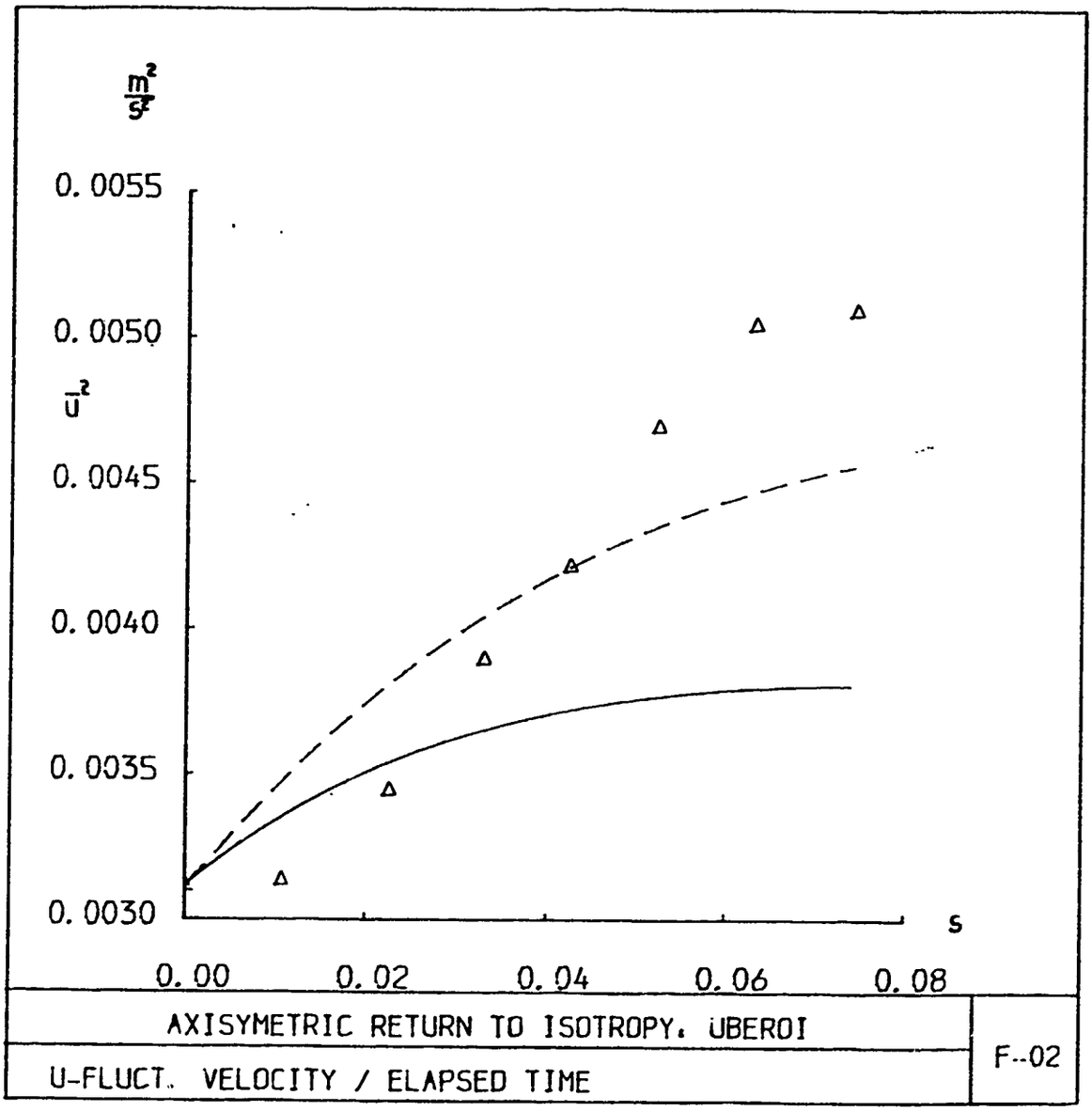

AXISYMETRIC RETURN TO ISOTROPY. UBEROI

U-FLUCT. VELOCITY / ELAPSED TIME

F--02

——— MODEL LRR

- - - - MODEL I

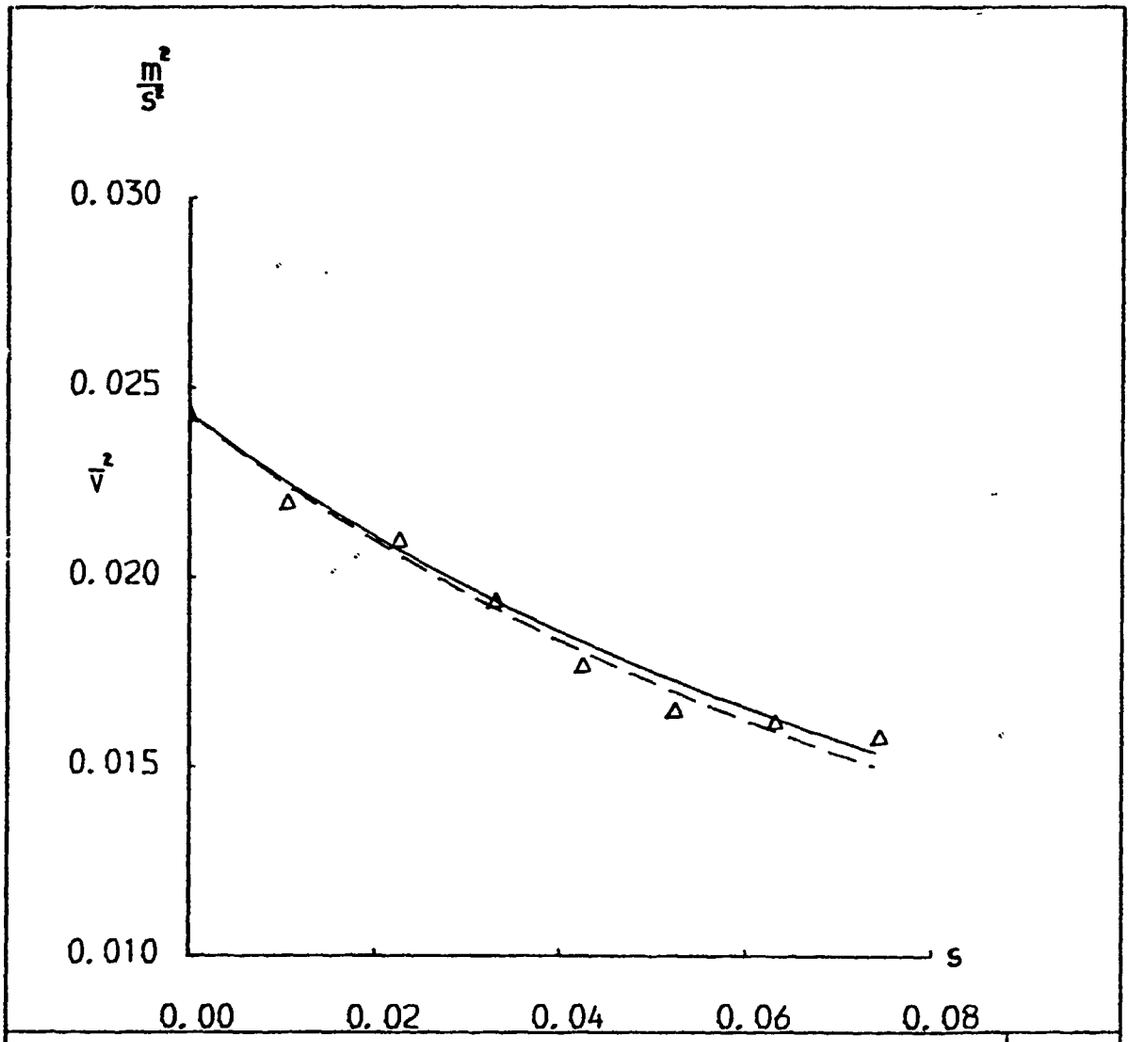

AXISYMETRIC RETURN TO ISOTROPY. UBEROI

V-FLUCT. VELOCITY / ELAPSED TIME

F-02

——— MODEL LRR

- - - - MODEL I

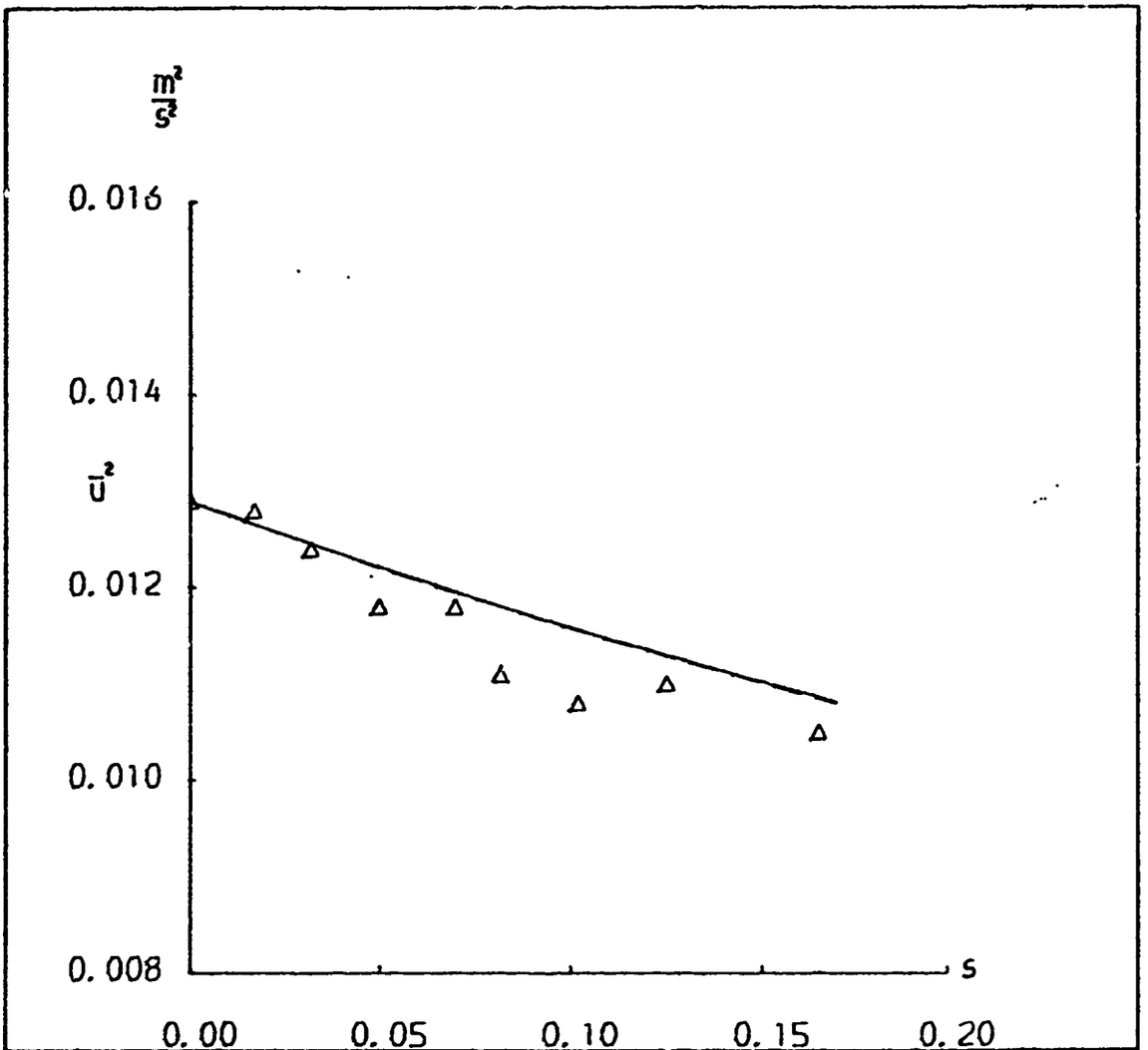

RETURN TO ISOTROPY. TUCKER & REYNOLDS

U-FLUCT. VELOCITY / ELAPSED TIME

F-03

_____ MODEL LRR

_ _ _ _ _ MODEL I

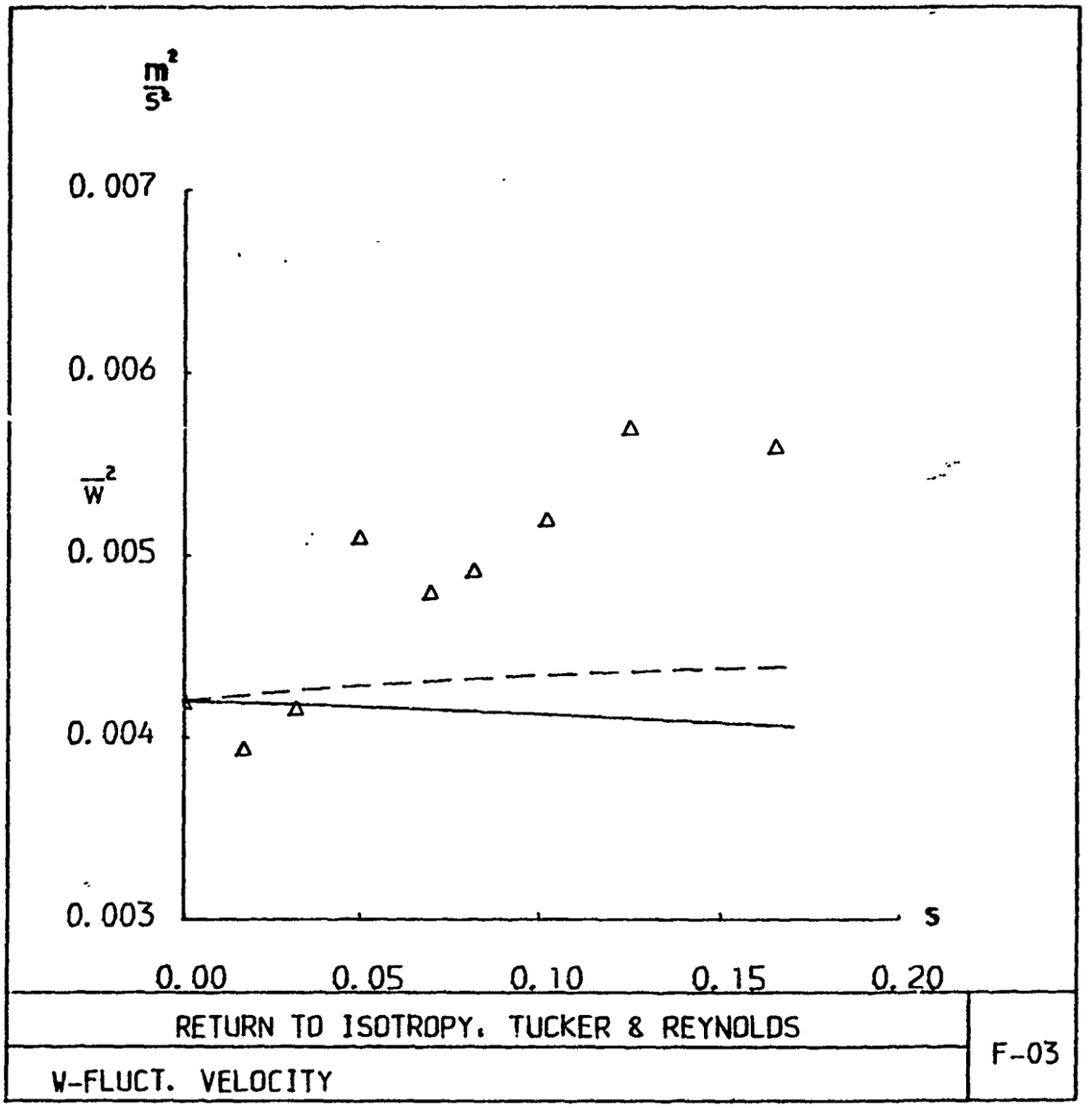

RETURN TO ISOTROPY. TUCKER & REYNOLDS

W-FLUCT. VELOCITY

F-03

MODEL LRR

MODEL I

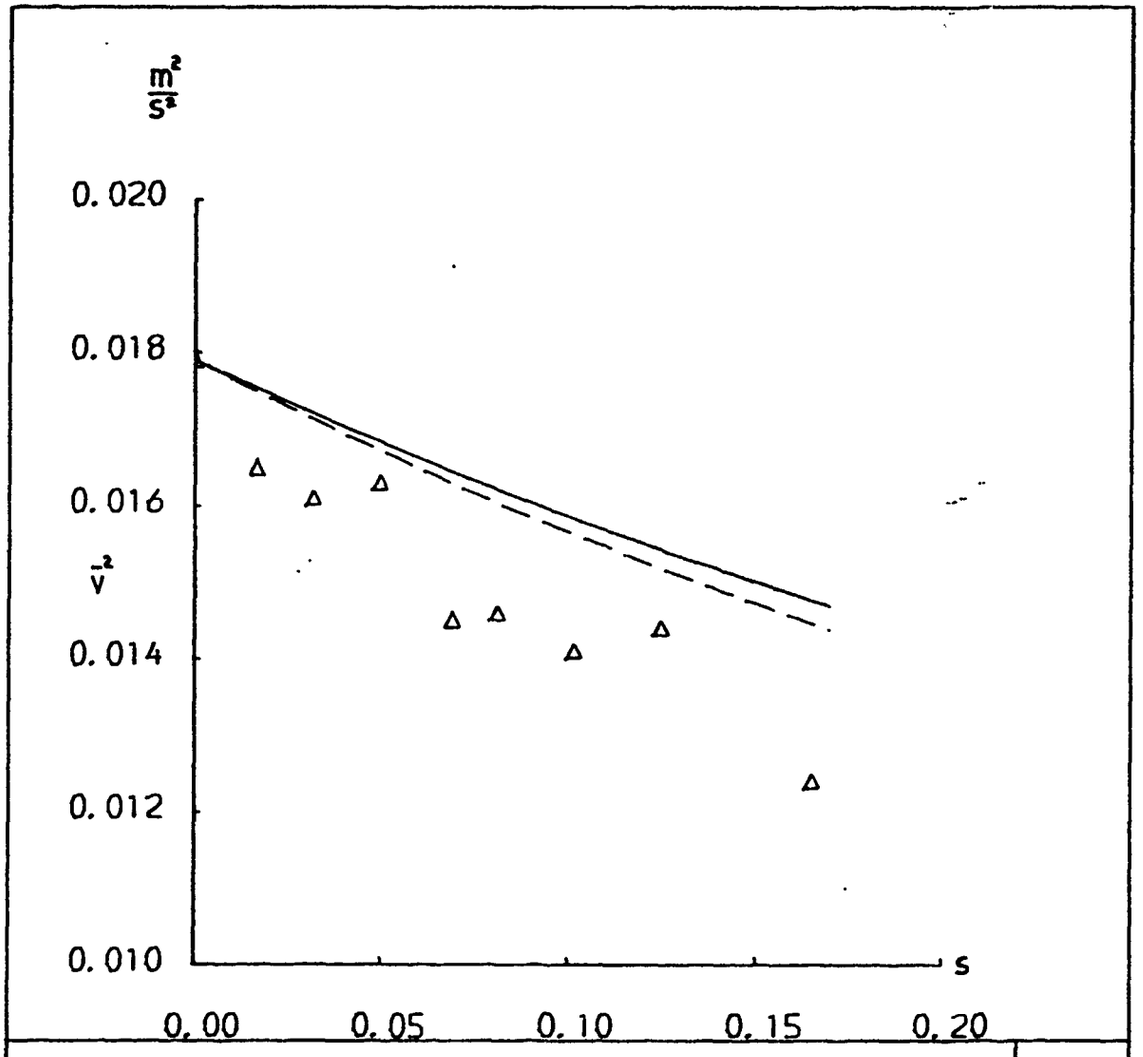

RETURN TO ISOTROPY. TUCKER & REYNOLDS

V-FLUCT. VELOCITY / ELAPSED TIME

F-03

MODEL LRR

MODEL I

MODEL II[1]

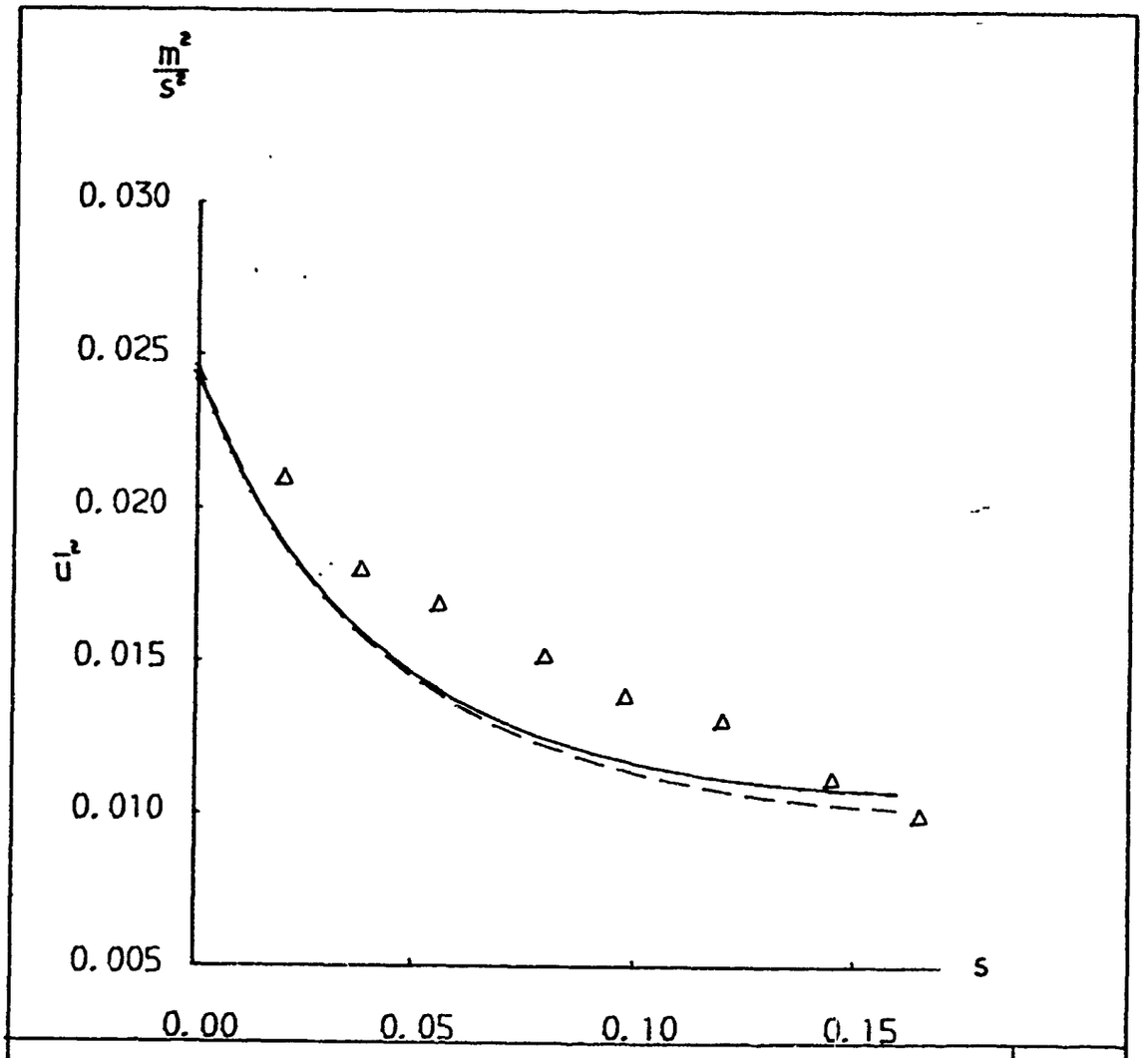

PLANE-STRAIN. TOWNSEND

U-FLUCT. VELOCITY / ELAPSED TIME

F-04

——— MODEL LRR

- - - - MODEL I

..... MODEL II[1]

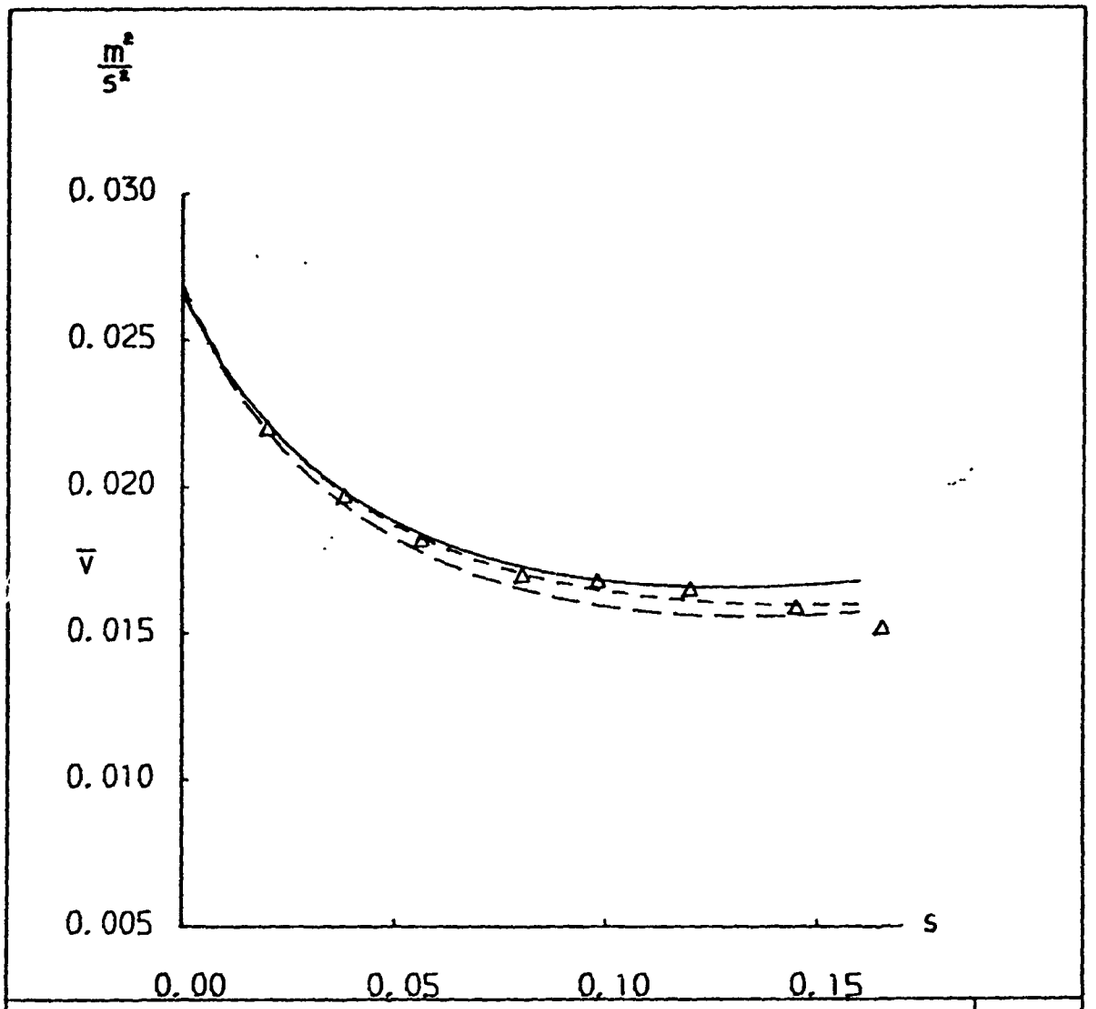

PLANE STRAIN: TOWNSEND

V-FLUCT. VELOCITY / ELAPSED TIME

F-04

——— MODEL LRR

– – – – – MODEL I

– – – – – MODEL II[0]

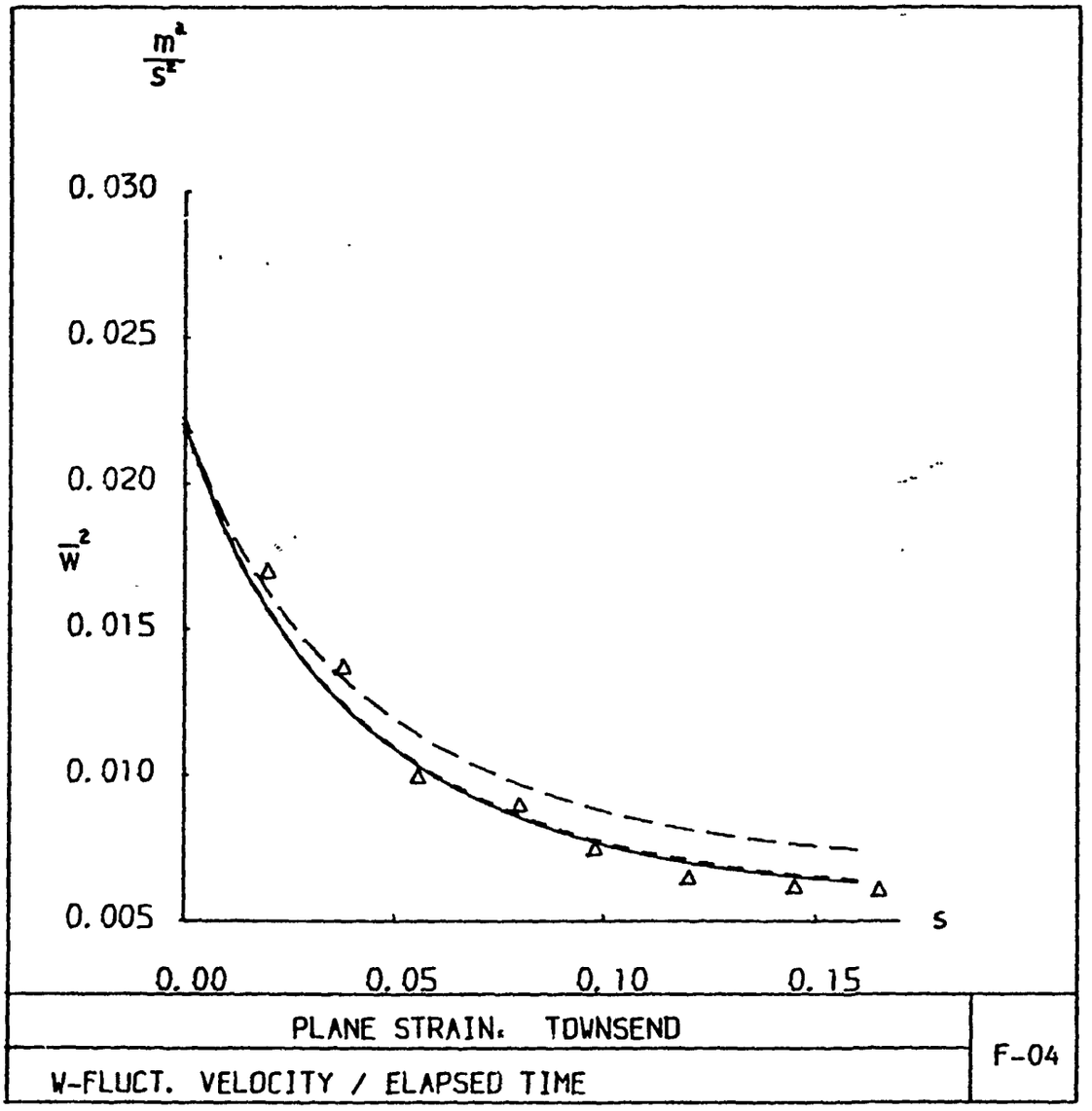

PLANE STRAIN. TOWNSEND

W-FLUCT. VELOCITY / ELAPSED TIME

F-04

MODEL LRR

MODEL I

MODEL III[1]

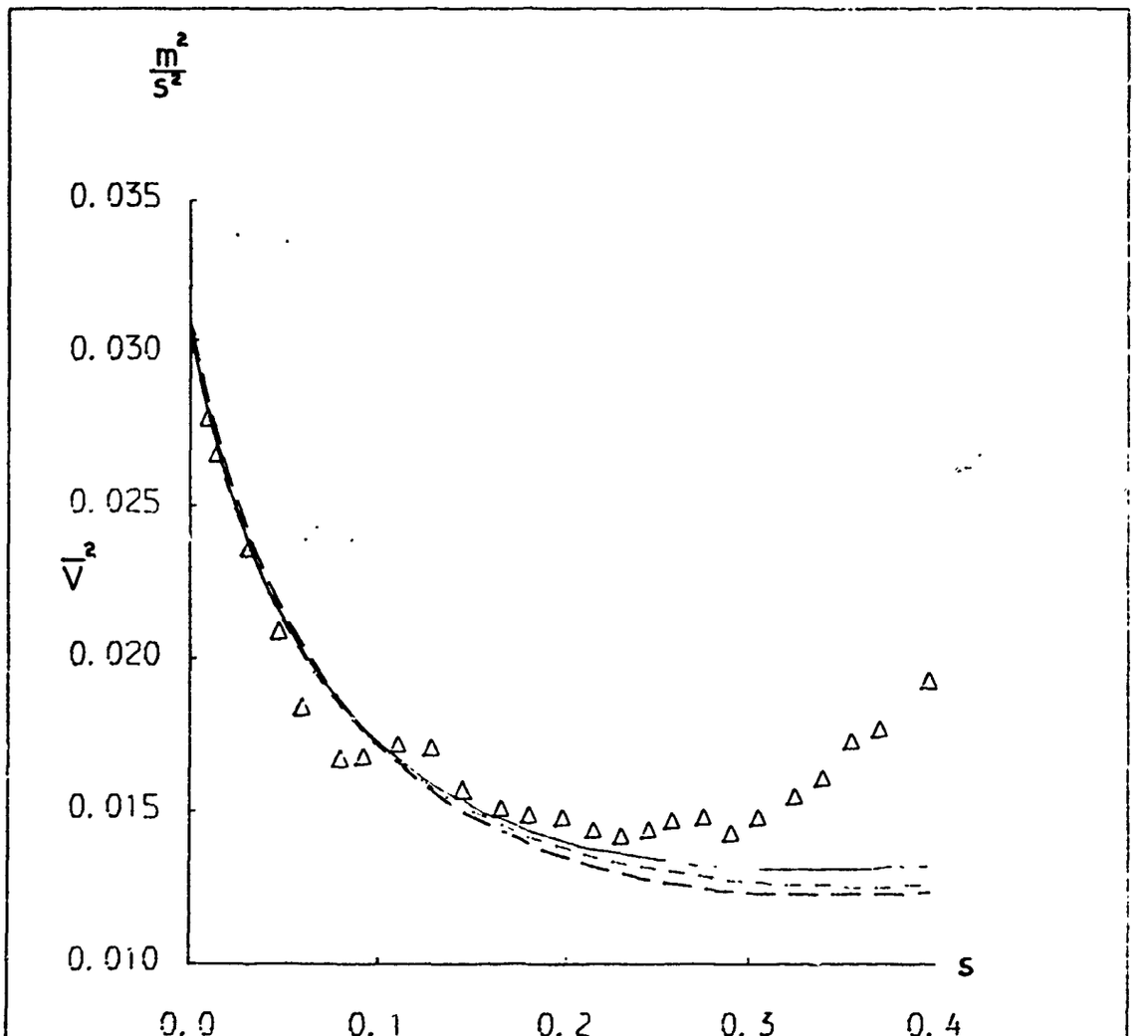

PLANE STRAIN. TUCKER & REYNOLDS	F-05
V-FLUCT. VELOCITY / ELAPSED TIME	

MODEL LRR

MODEL II(1)

MODEL I

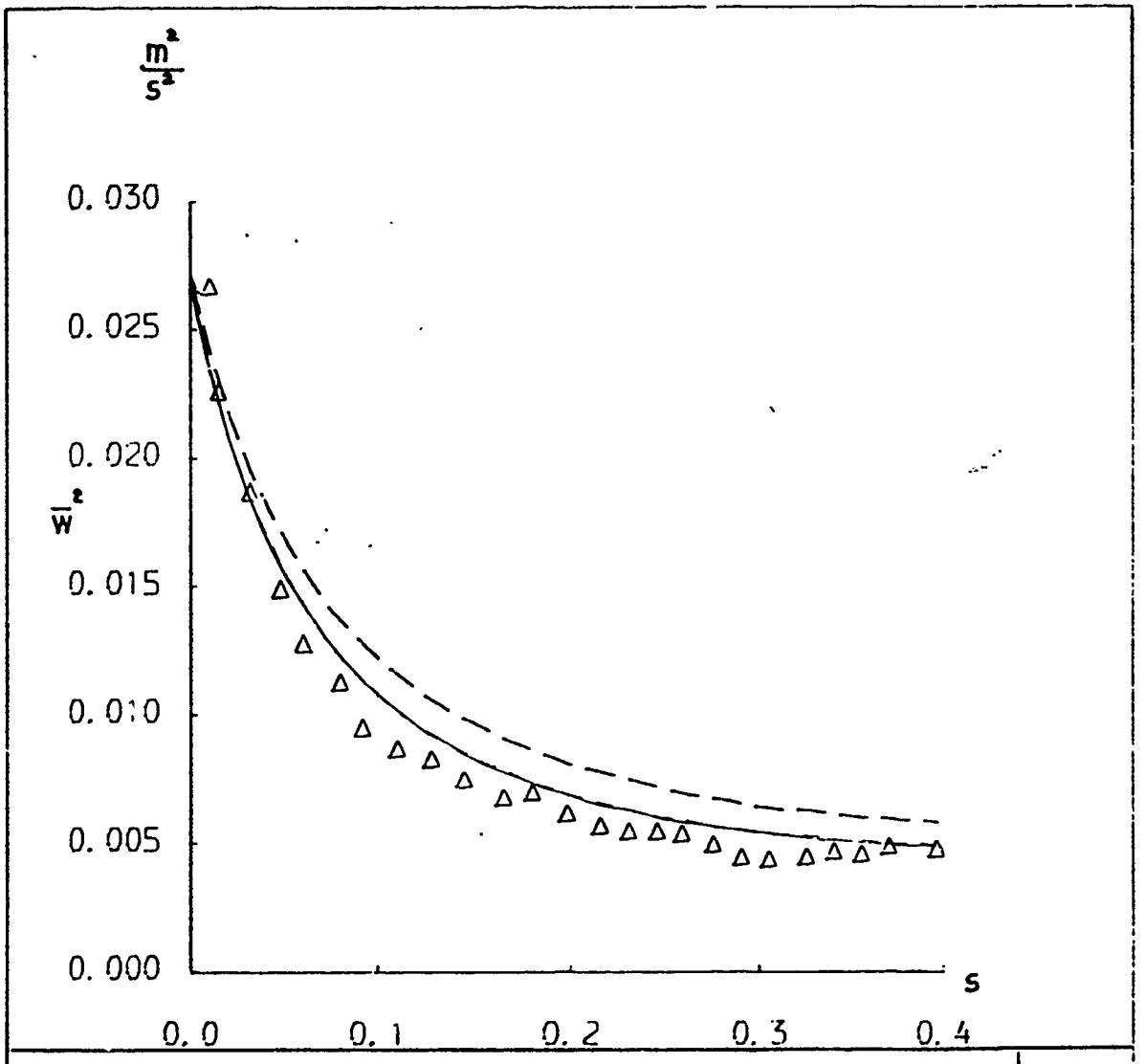

PLANE STRAIN. TUCKER & REYNOLDS

W-FLUCT. VELOCITY / ELAPSED TIME

F-05

——— MODEL LRR

_ _ _ _ _ MODEL I

_ _ _ _ _ _ MODEL II(1)

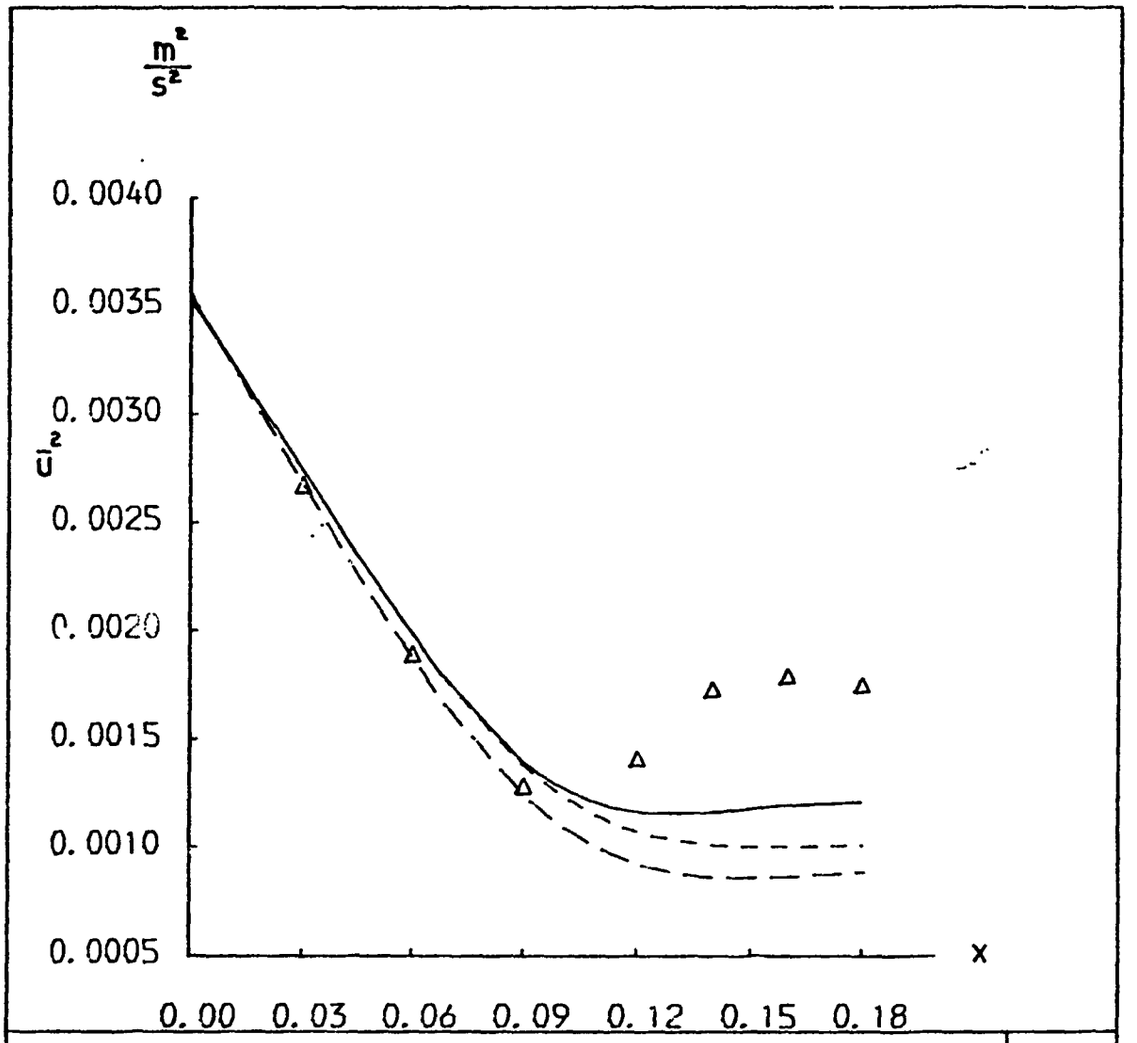

AXISYMETRIC STRAIN. TAN-ATICHAT

U-FLUCT. VELOCITY / DISTANCE

F-06

——— MODEL LRR

– – – – – MODEL I

– – – – – – – MODEL II(1)

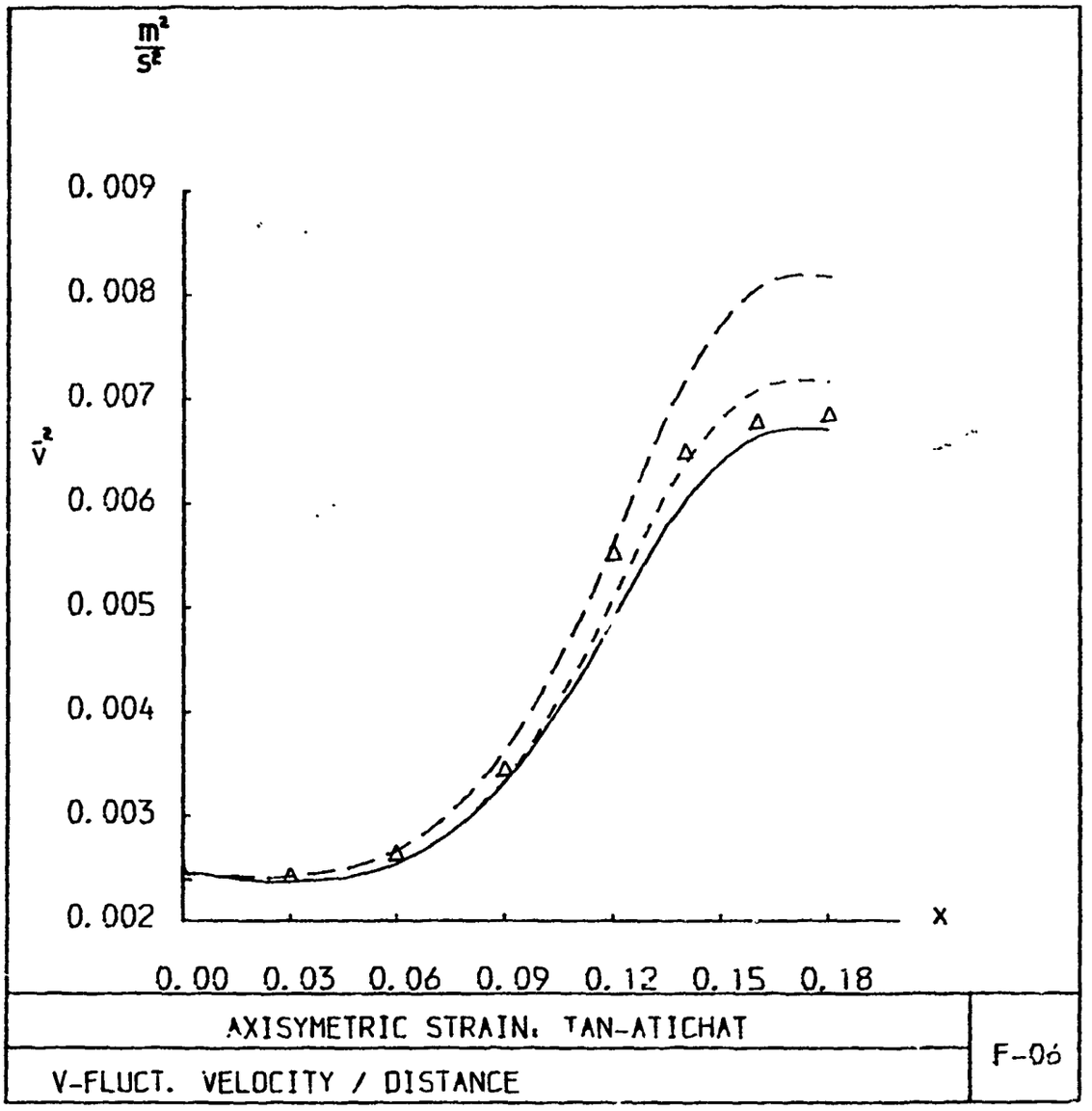

AXISYMETRIC STRAIN: TAN-ATICHAT

V-FLUCT. VELOCITY / DISTANCE

F-06

_____ MODEL LRR

_ _ _ _ _ MODEL I

_ _ _ _ _ _ MODEL II(t)

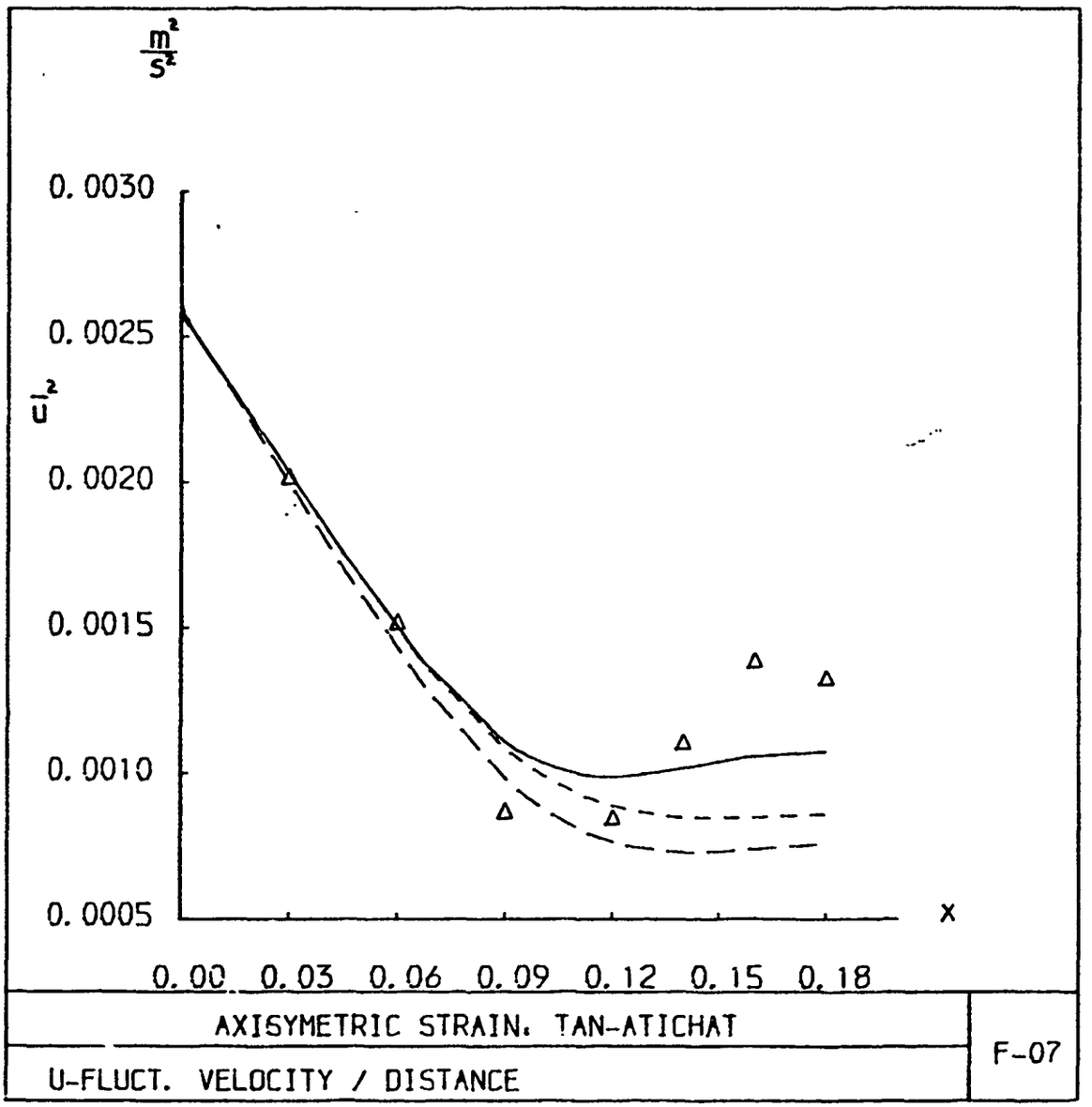

AXISYMETRIC STRAIN. TAN-ATICHAT

U-FLUCT. VELOCITY / DISTANCE

F-07

MODEL LRR

MODEL I

MODEL II(1)

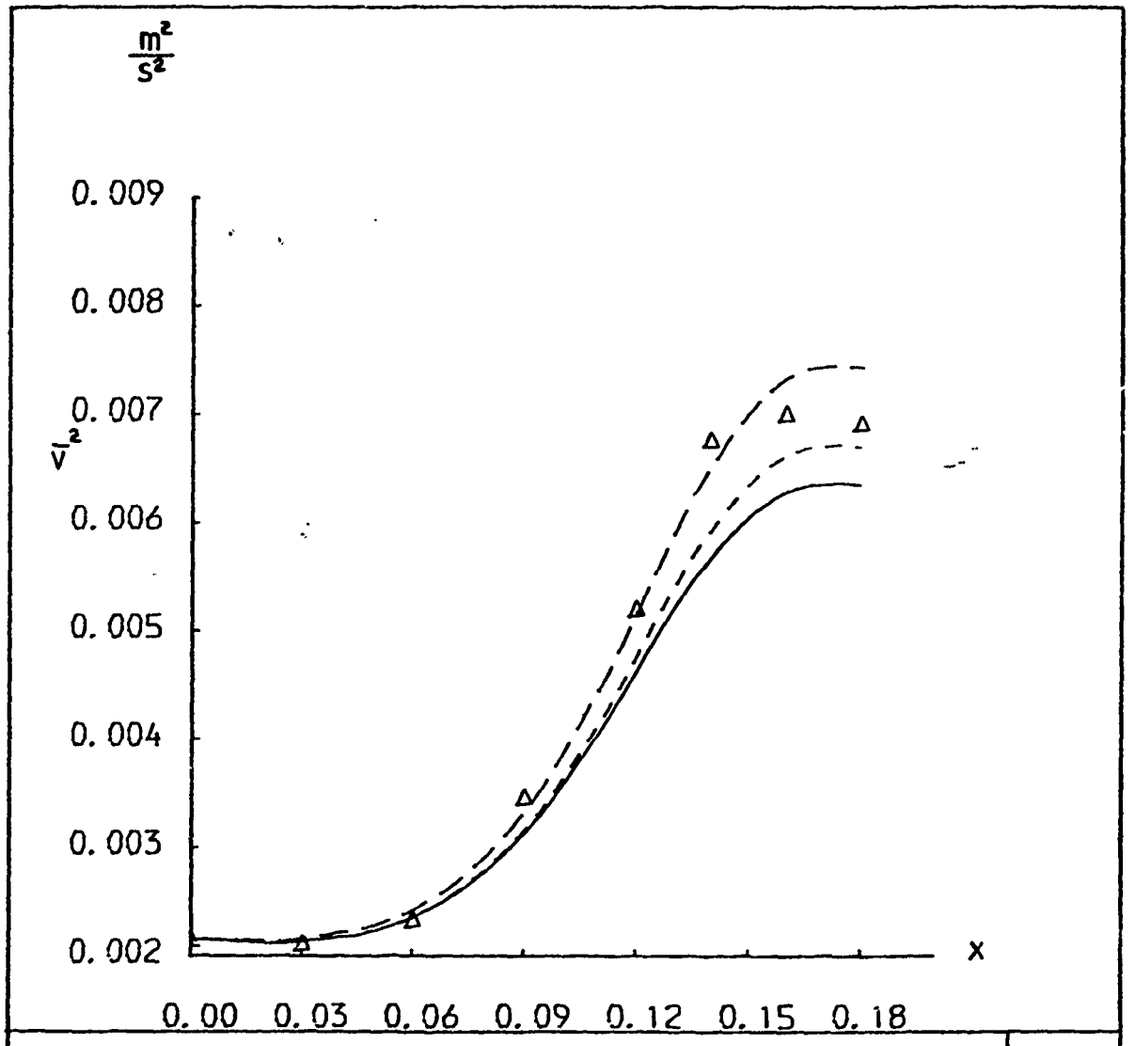

AXISYMETRIC STRAIN. TAN-ATICHAT

V-FLUCT. VELOCITY / DISTANCE

F-07

_____ MODEL LRR

_ _ _ _ _ MODEL I

_ _ _ _ _ MODEL II(1)

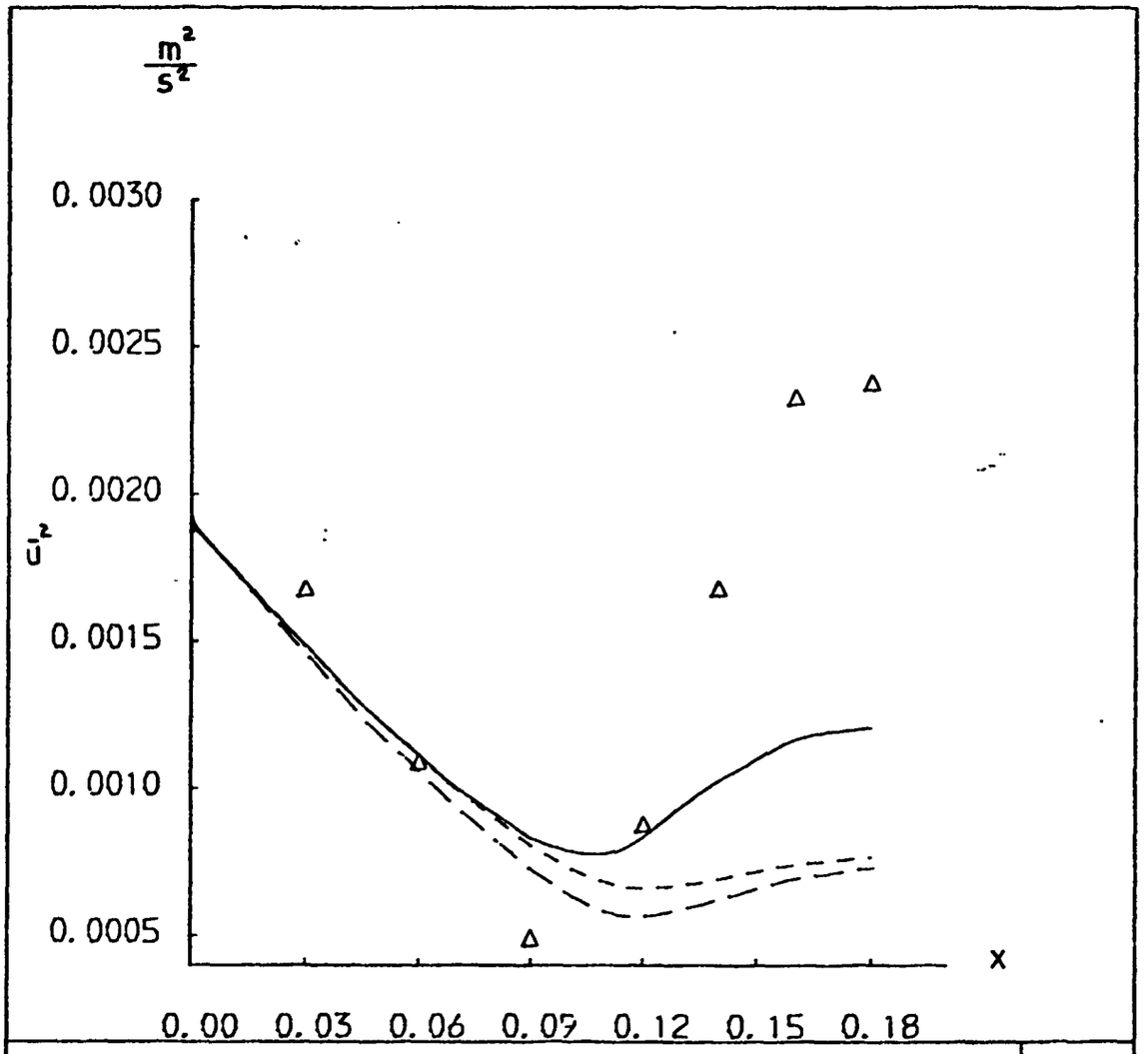

AXISYMETRIC STRAIN. TAN-ATICHAT

U-FLUCT. VELOCITY / DISTANCE

F-08

——— MODEL LRR

– – – – MODEL I

– – – – – – MODEL II(1)

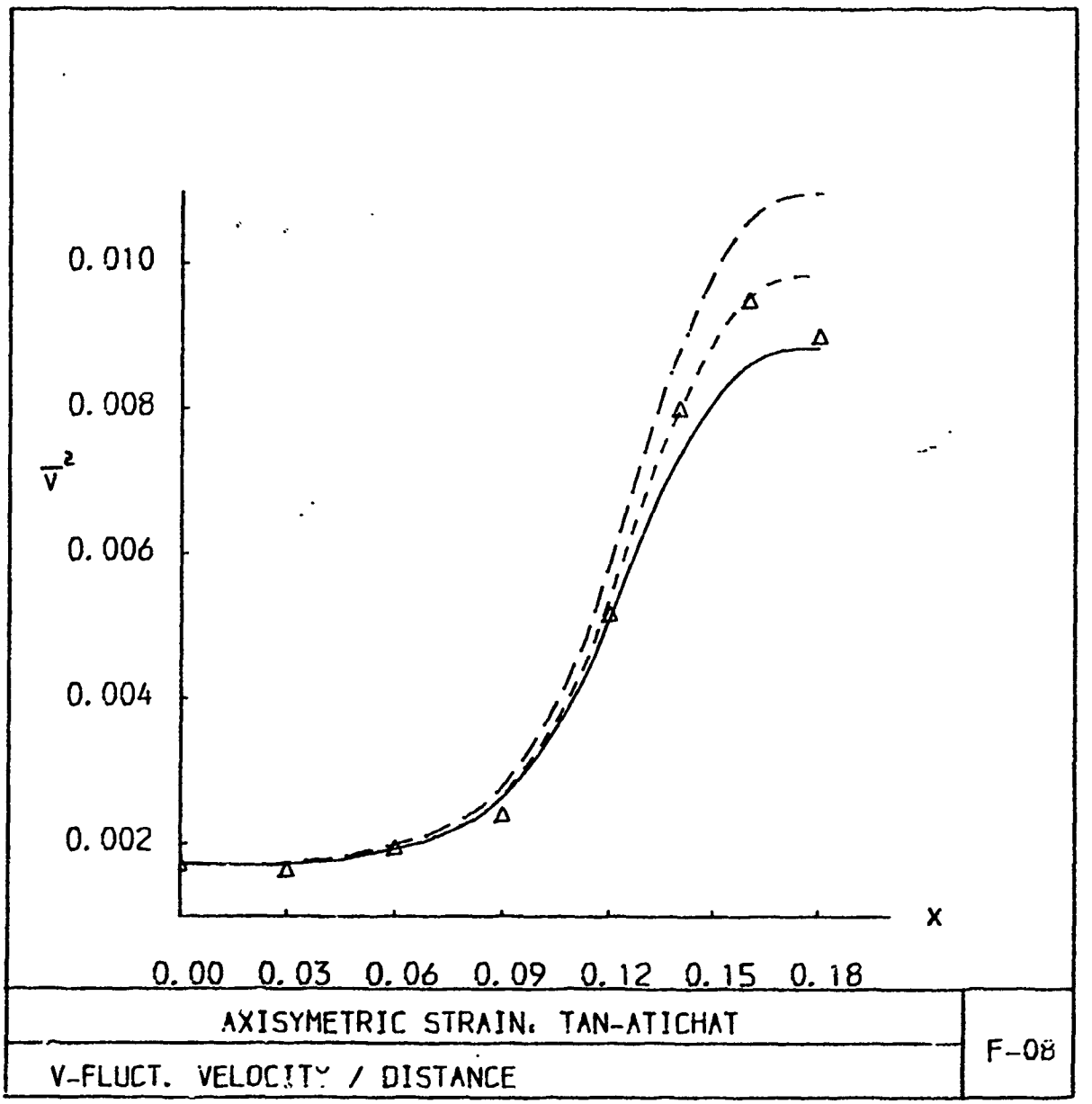

AXISYMETRIC STRAIN. TAN-ATICHAT

V-FLUCT. VELOCITY / DISTANCE

F-08

———— MODEL LRR

– – – – MODEL I

– – – – MODEL II(t)

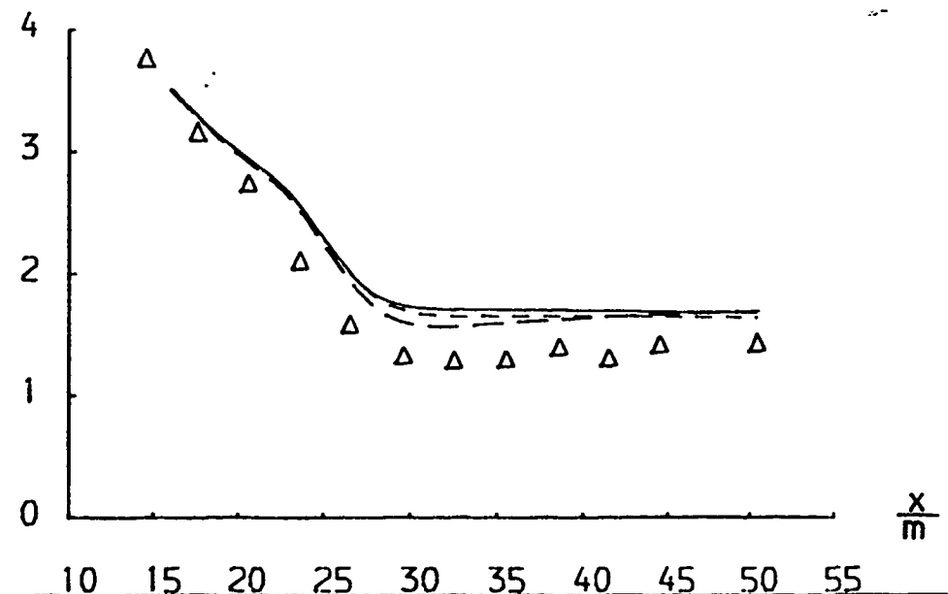

AXISYMETRIC STRAIN, UBEROI

NORM. U-FLUCT. VELOCITY / NORM. DISTANCE

F-09

——— MODEL LRR

– – – – – MODEL I

—.—.— MODEL II(1)

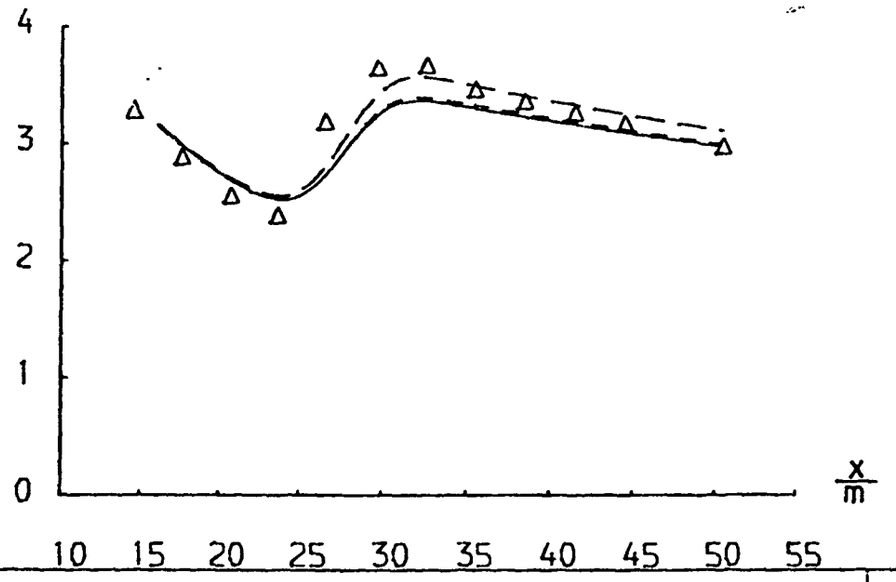

AXISYMETRIC STRAIN. UBEROI

NORM. V-FLUCT. VELOCITY / NORM. DISTANCE

F-09

MODEL LRR

MODEL I

MODEL II[1]

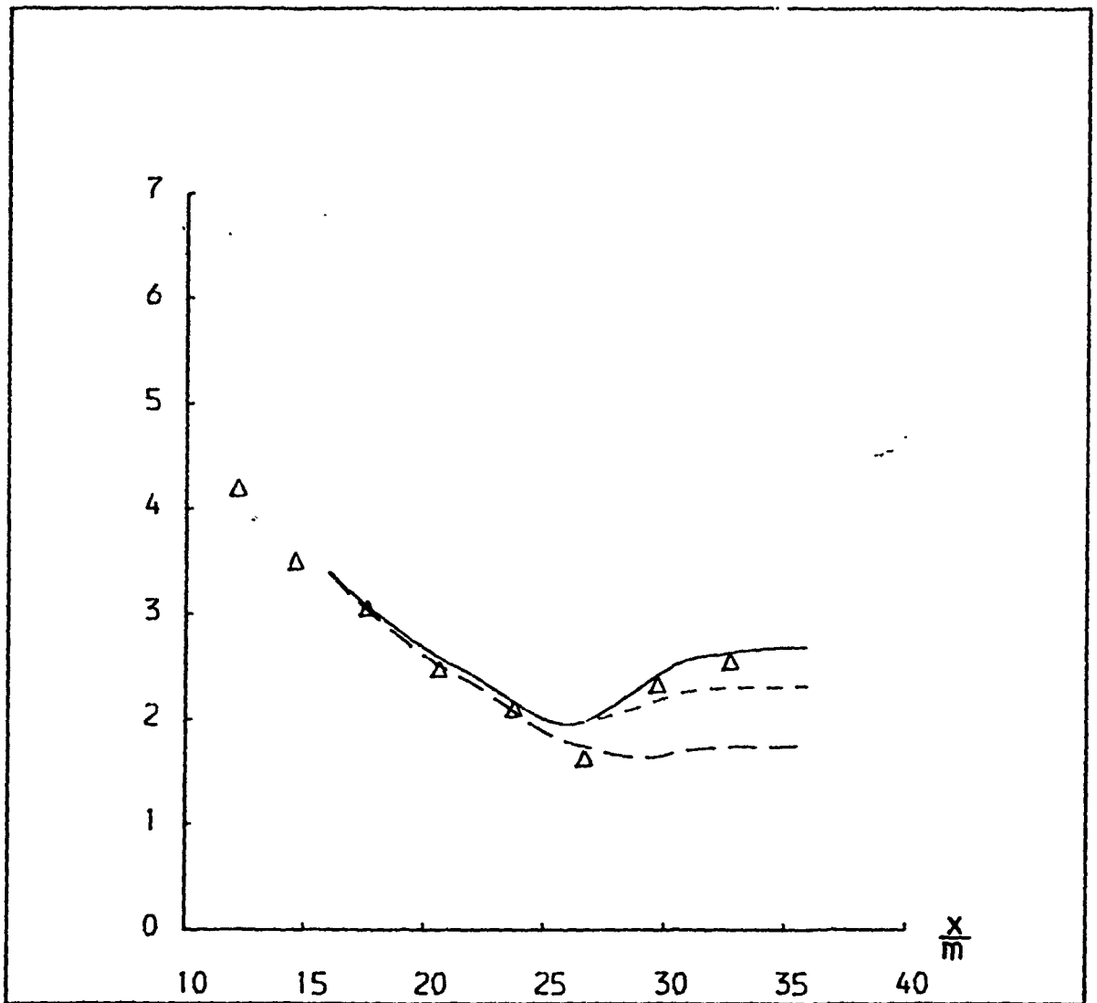

AXISYMETRIC STRAIN: UBEROI

NORM. U-FLUCT. VELOCITY / NORM. DISTANCE

F-10

_____ MODEL LRR

_ _ _ _ _ MODEL I

_ . _ . _ MODEL II(1)

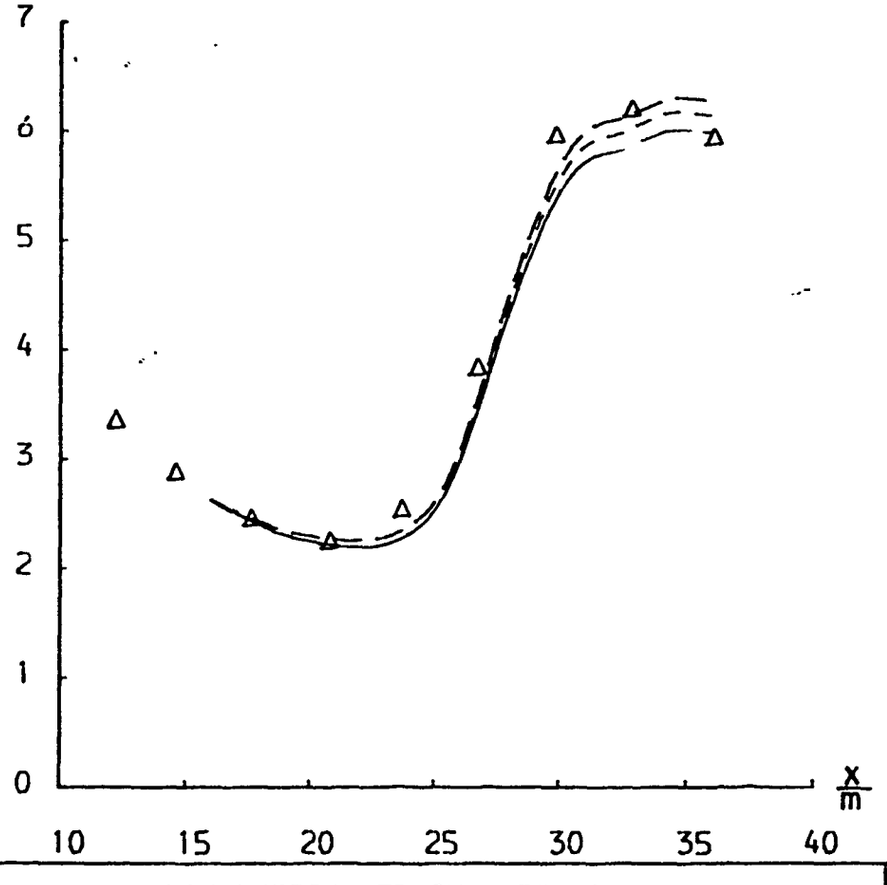

AXISYMETRIC STRAIN. UBEROI

NORM. V-FLUCT. VELOCITY / NORM. DISTANCE

F-10

MODEL LRR

MODEL I

MODEL II(1)

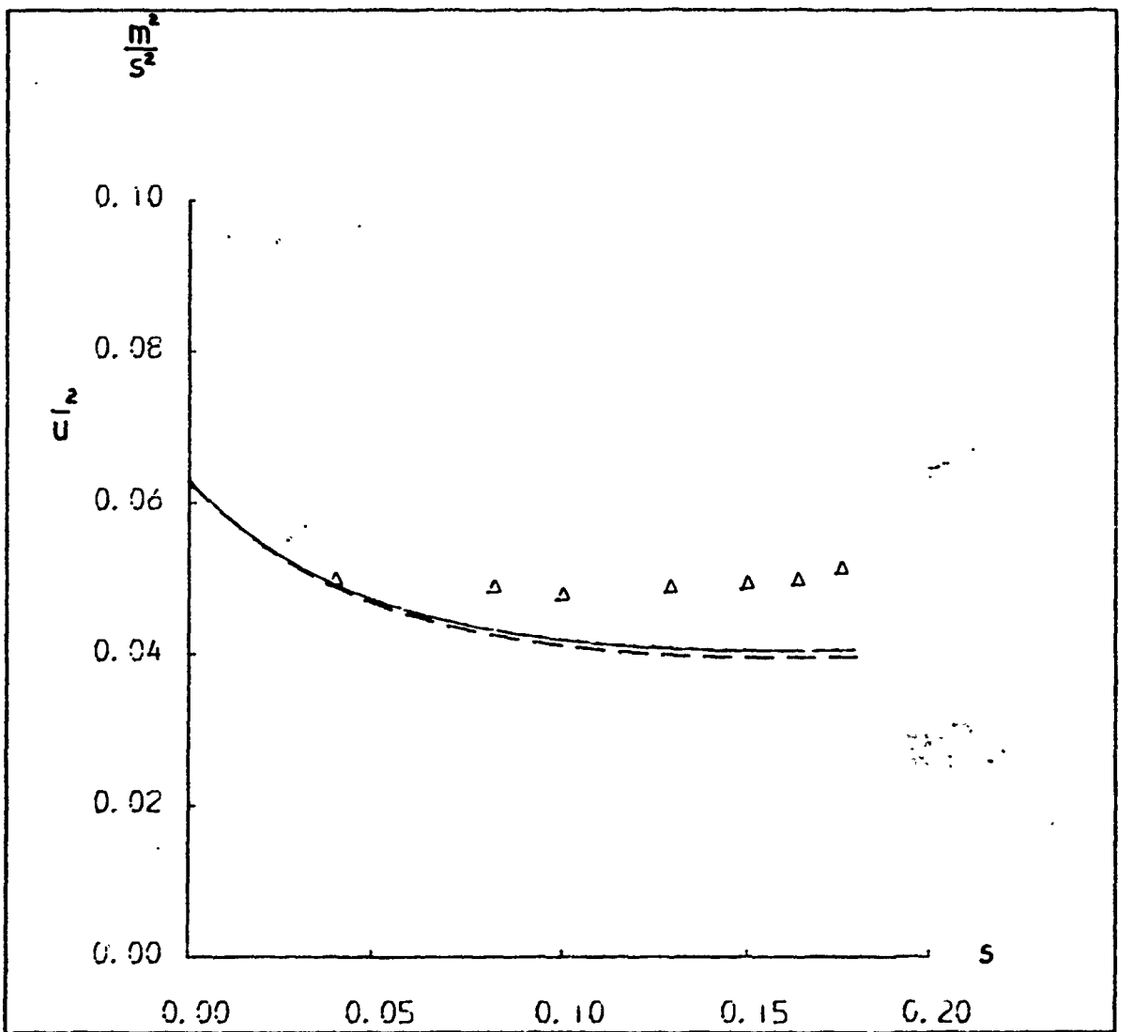

SHEARED TURBULENCE CHC-FLOW

U-FLUCT. VELOCITY / ELAPSED T

F-11

——— MODEL LRR

– – – – – MODEL I

– – – – – – MODEL II(1)

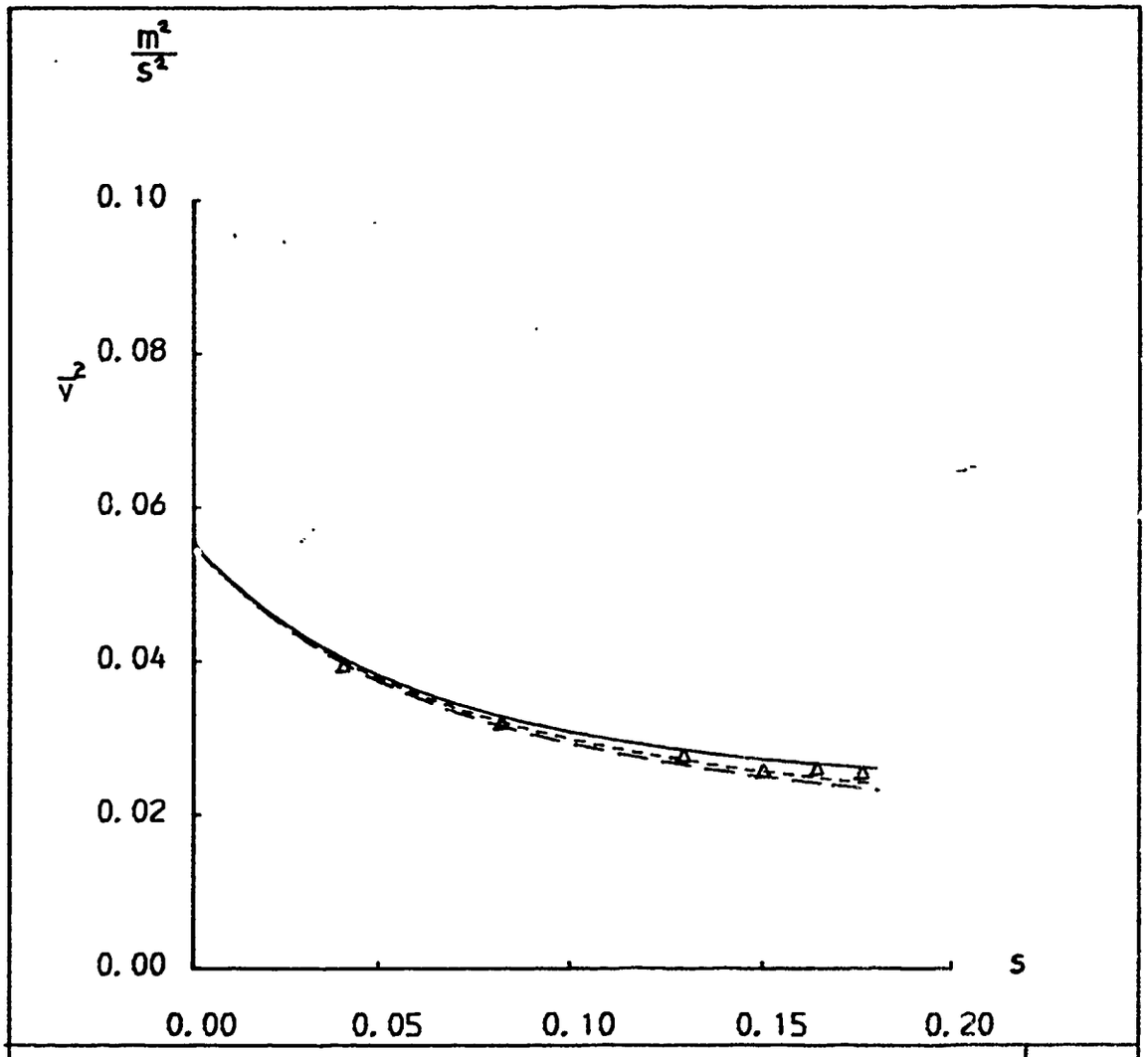

SHEARED TURBULENCE CHC-FLOW

V-FLUCT VELOCITY / ELAPSED TIME

F-11

——— MODEL LRR

– – – – – MODEL I

– – – – – MODEL II(1)

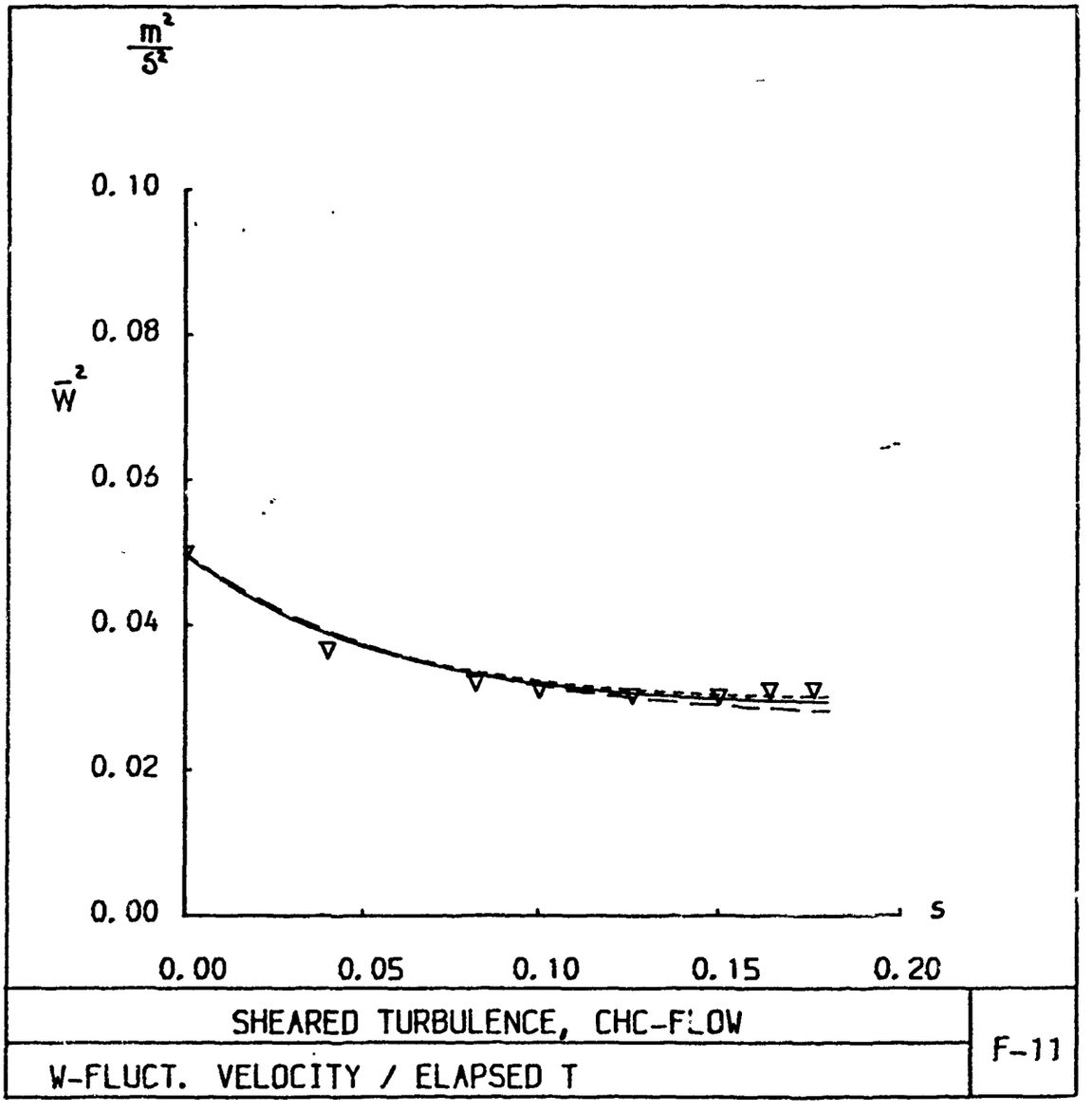

SHEARED TURBULENCE, CHC-FLOW

W-FLUCT. VELOCITY / ELAPSED T

F-11

——— MODEL LRR

— — — — MODEL I

—·—·— MODEL II(1)

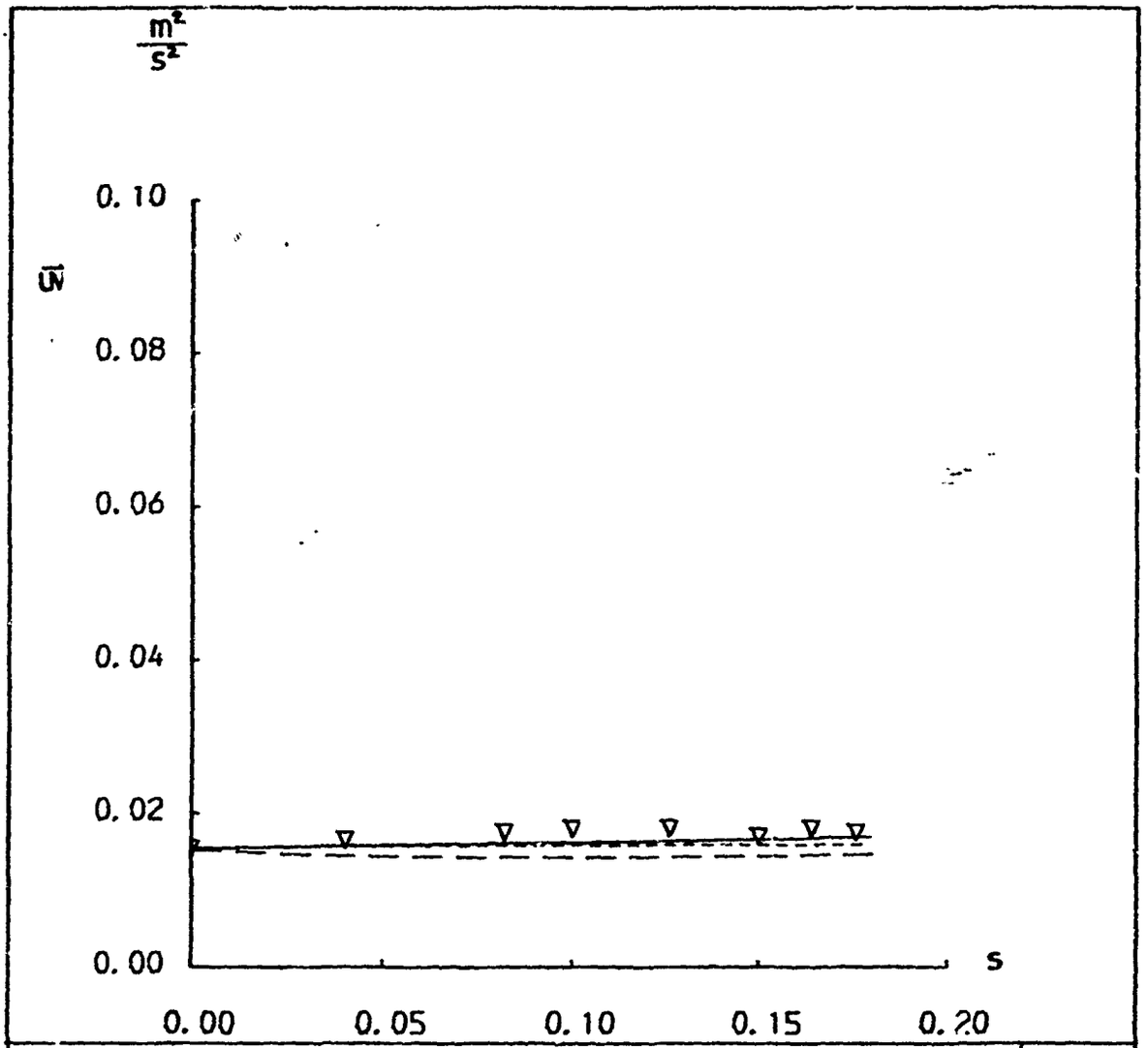

SHEARED TURBULENCE, CHC-FLOW

UV-FLUCT. VELOCITY / ELAPSED TIME

F-11

_____ MODEL LRR

_ _ _ _ _ MODEL I

_ _ _ _ _ _ MODEL II(1)

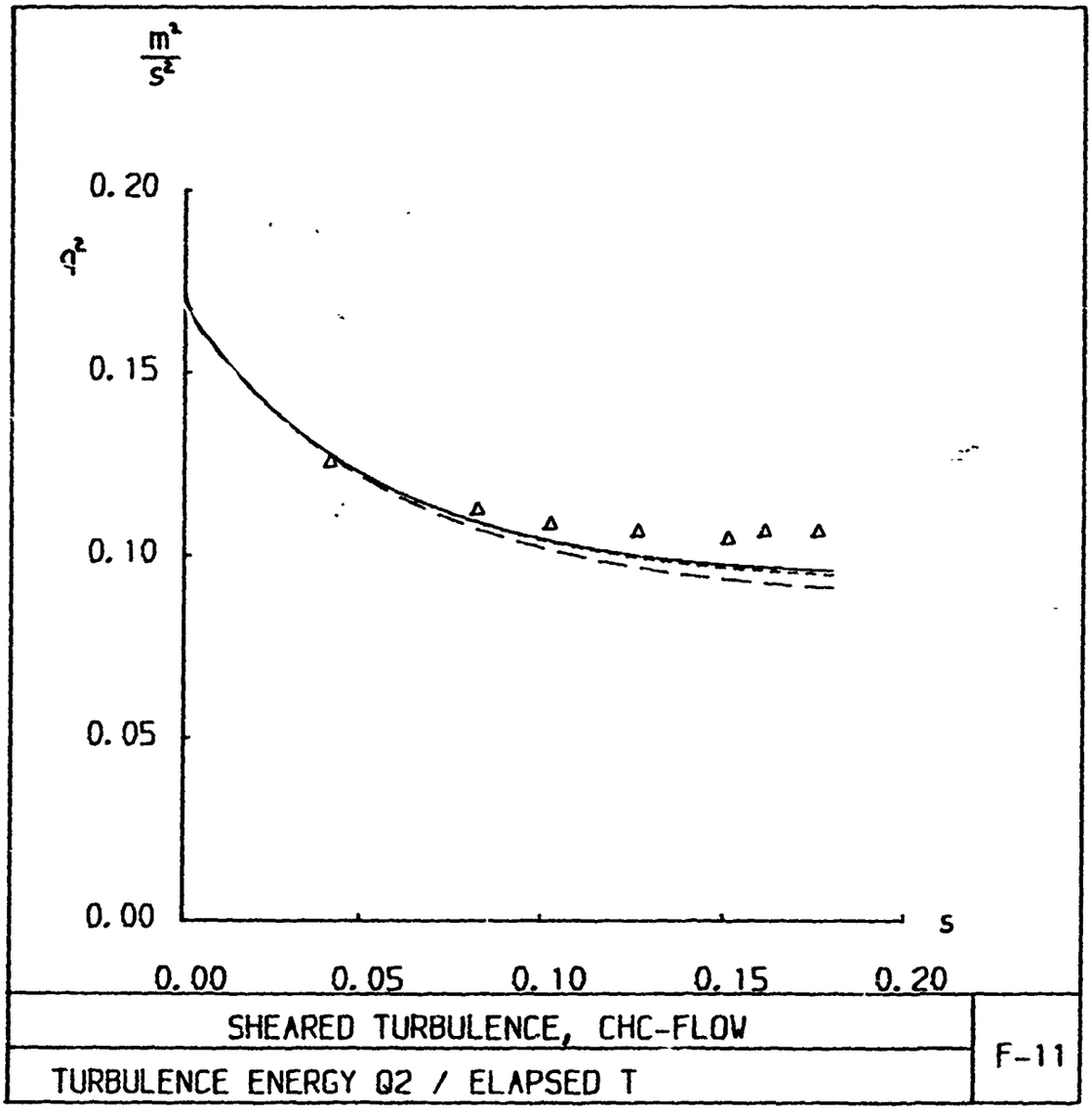

SHEARED TURBULENCE, CHC-FLOW

TURBULENCE ENERGY Q2 / ELAPSED T

F-11

MODEL LRR

MODEL II(1)

MODEL I

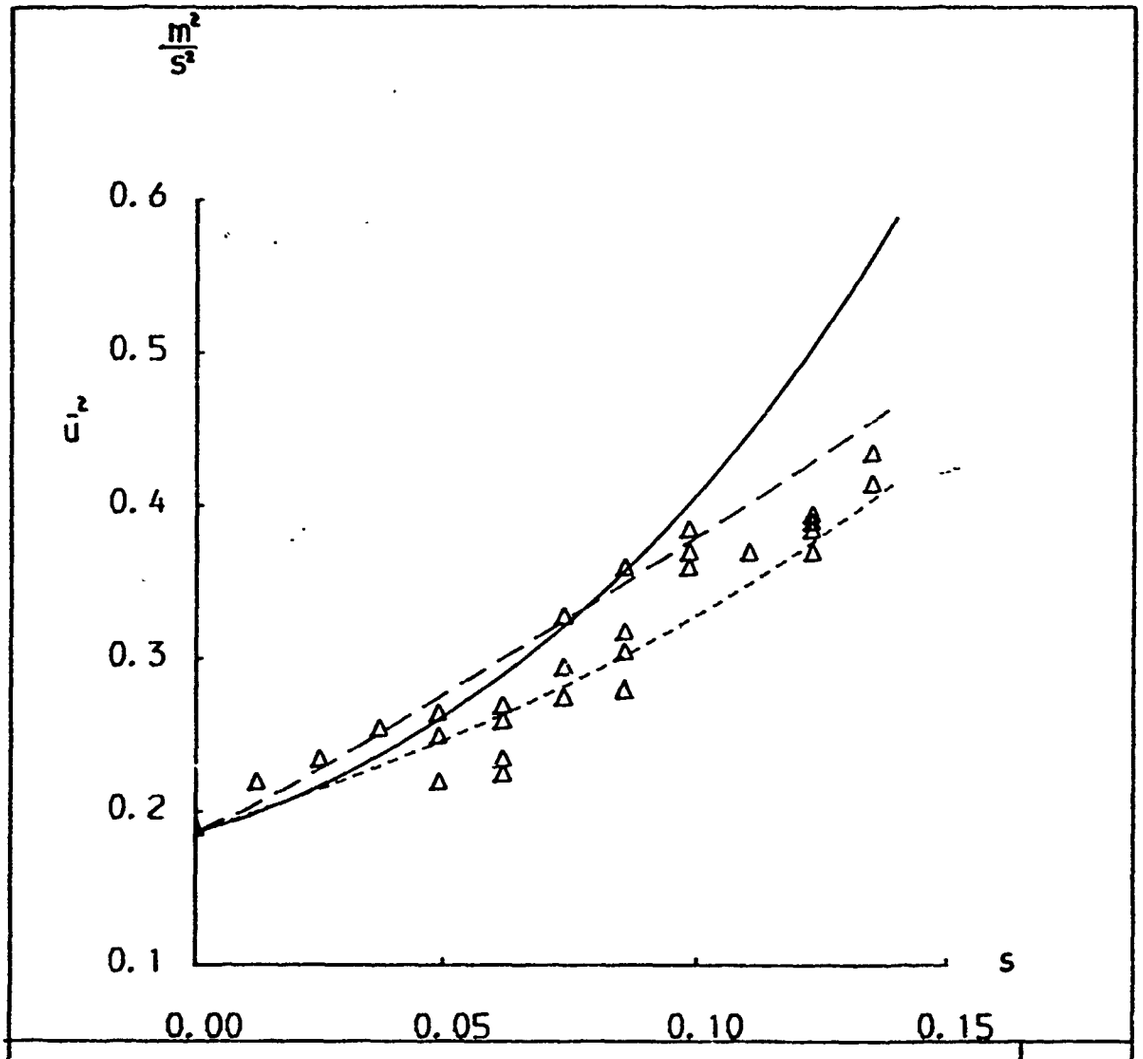

SHEARED TURBULENCE, HGC-FLOW

U-FLUCT. VELOCITY / ELAPSED TIME

F-12

——— MODEL LRR

– – – – – MODEL I

– – – – – MODEL IIa)

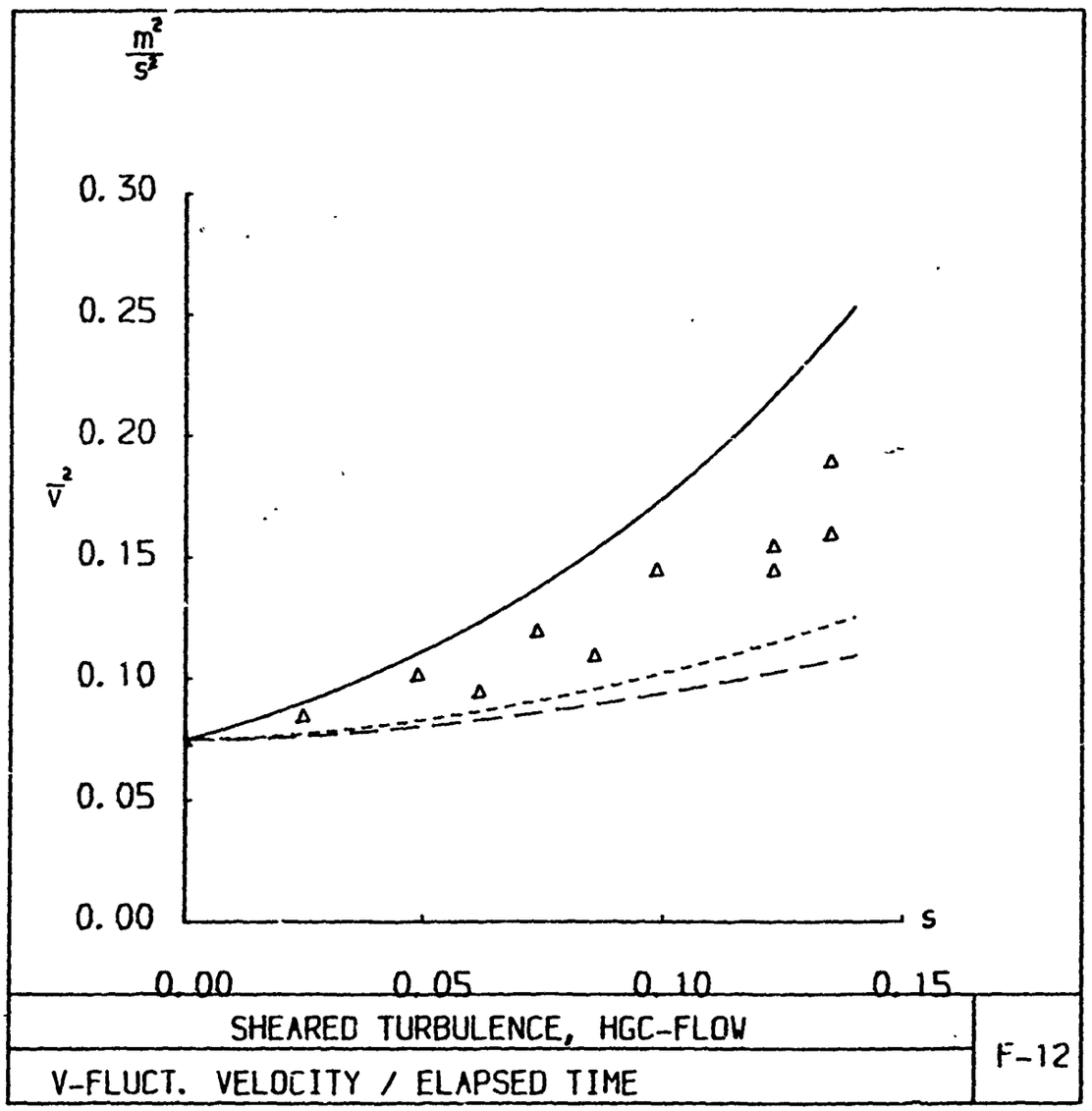

SHEARED TURBULENCE, HGC-FLOW

V-FLUCT. VELOCITY / ELAPSED TIME

F-12

———— MODEL LRR

– – – – – MODEL I

— · · · · · MODEL III)

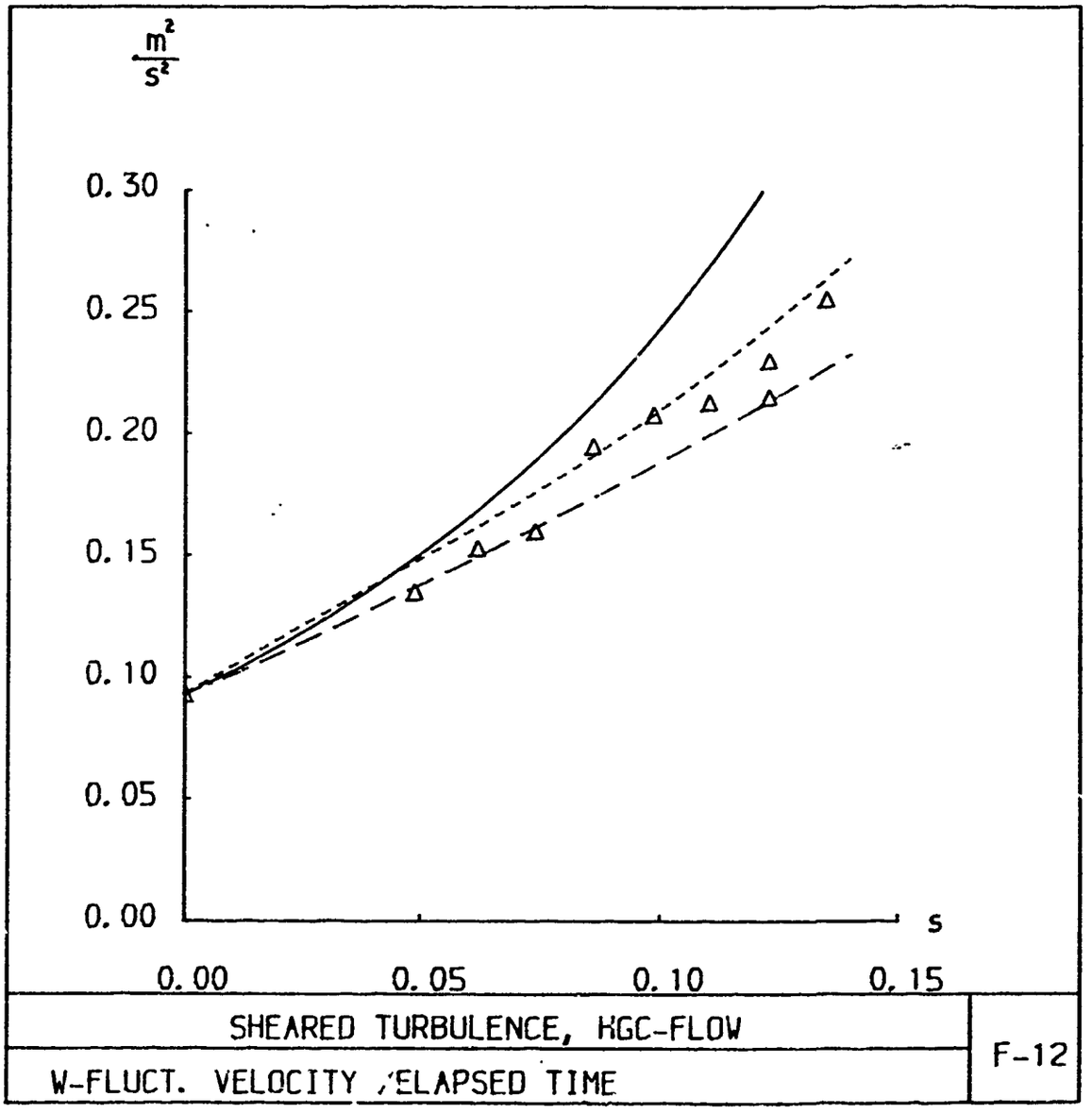

SHEARED TURBULENCE, KGC-FLOW

W-FLUCT. VELOCITY / ELAPSED TIME

F-12

——— MODEL LRR

_ _ _ _ _ MODEL I

. . . . . MODEL II(1)

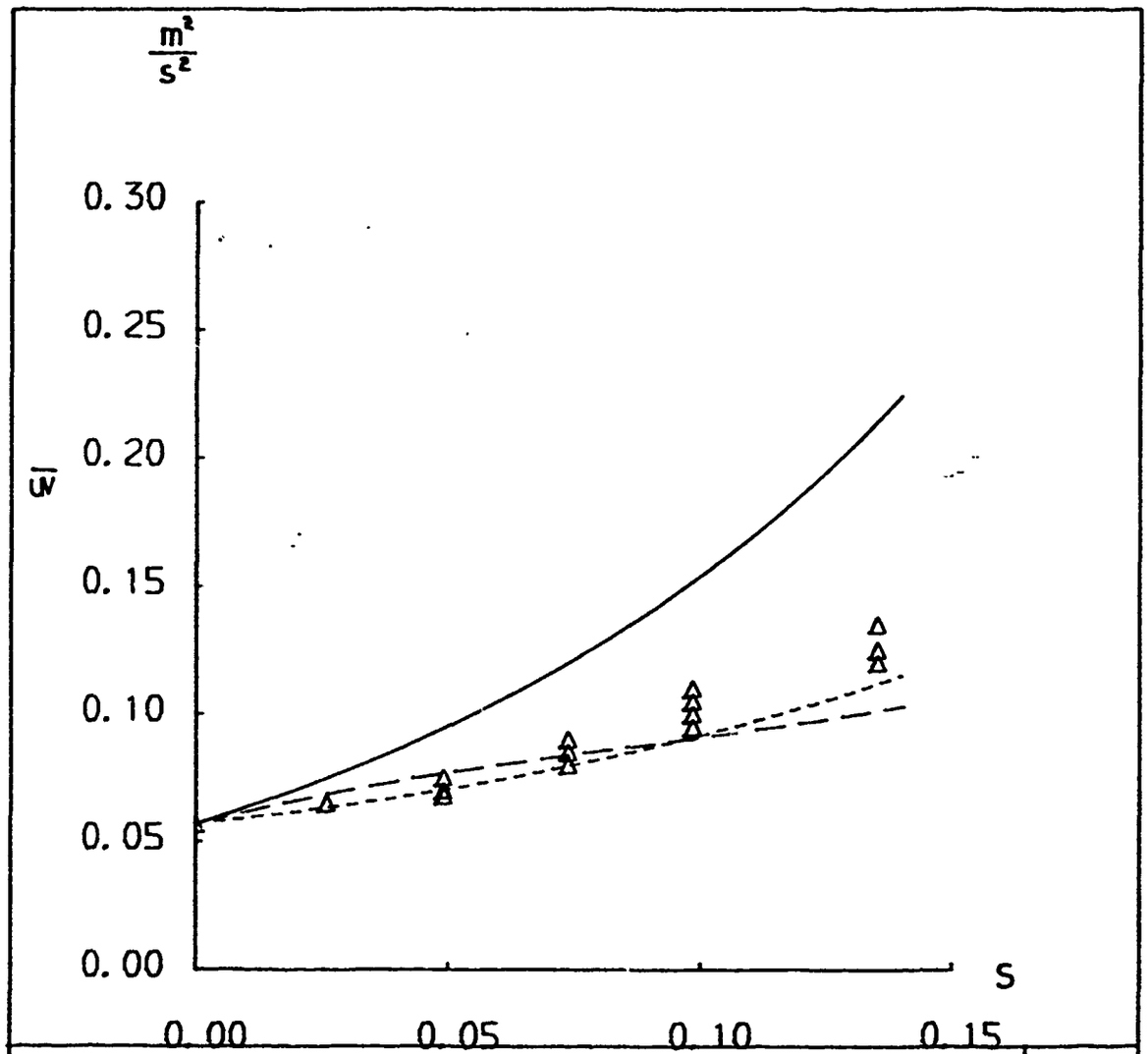

SHEARED TURBULENCE, HGC-FLOW

UV-REYNOLDS STRESS / ELAPSED TIME

F-12

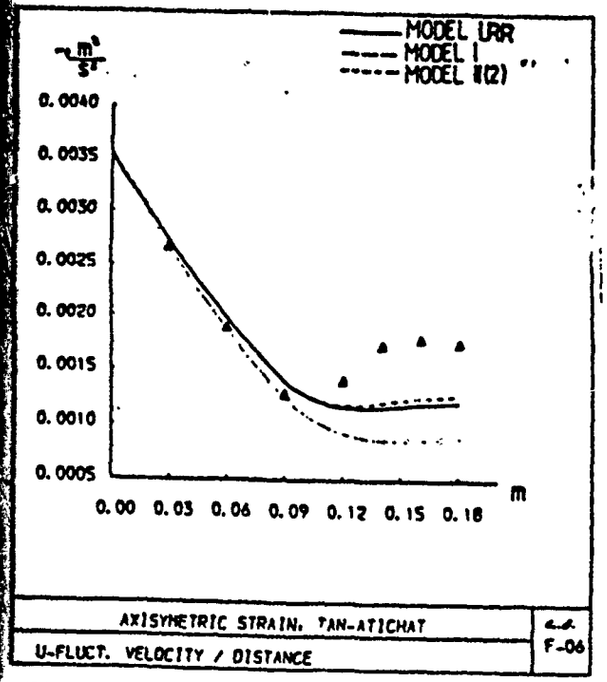
MODEL LRR
MODEL I
MODEL II(2)
m²/s²
0.0040
0.0035
0.0030
0.0025
0.0020
0.0015
0.0010
0.0005
0.00 0.03 0.06 0.09 0.12 0.15 0.18
m
AXISYMETRIC STRAIN, TAN-ATICHAT
U-FLUCT. VELOCITY / DISTANCE
F-06

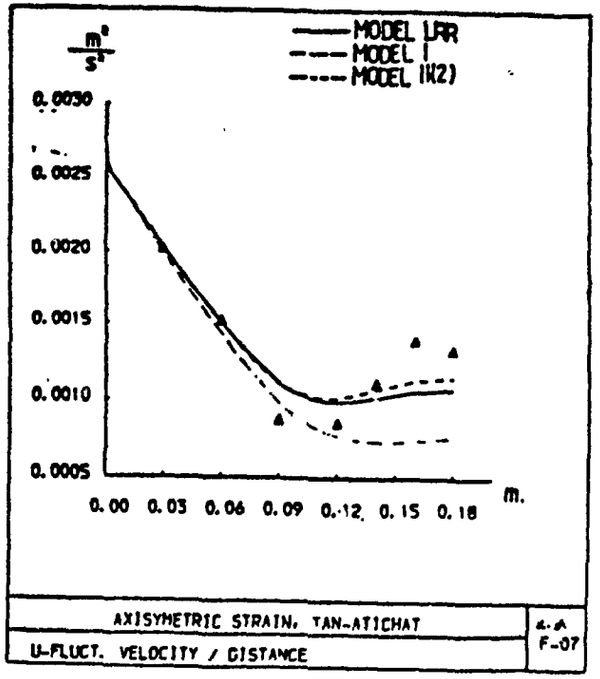
MODEL LRR
MODEL I
MODEL II(2)
m²/s²
0.0030
0.0025
0.0020
0.0015
0.0010
0.0005
0.00 0.03 0.06 0.09 0.12 0.15 0.18
m.
AXISYMETRIC STRAIN, TAN-ATICHAT
U-FLUCT. VELOCITY / DISTANCE
F-07

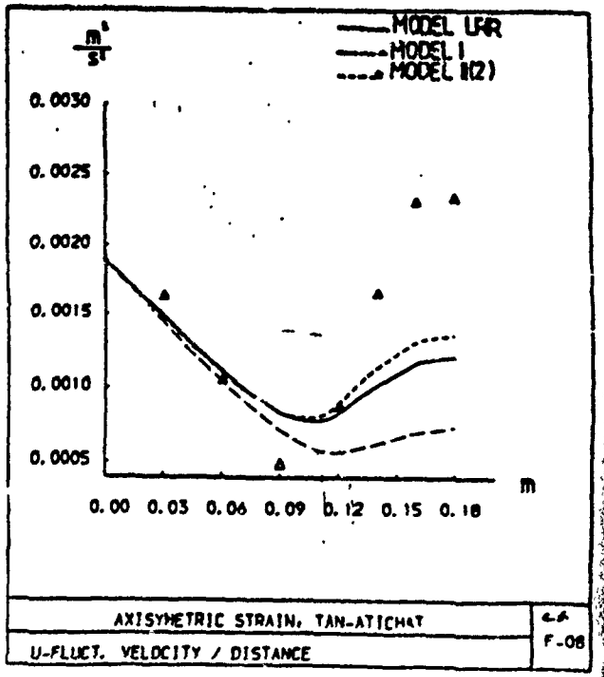
MODEL LRR
MODEL I
MODEL II(2)
m²/s²
0.0030
0.0025
0.0020
0.0015
0.0010
0.0005
0.00 0.03 0.06 0.09 0.12 0.15 0.18
m
AXISYMETRIC STRAIN, TAN-ATICHAT
U-FLUCT. VELOCITY / DISTANCE
F-08

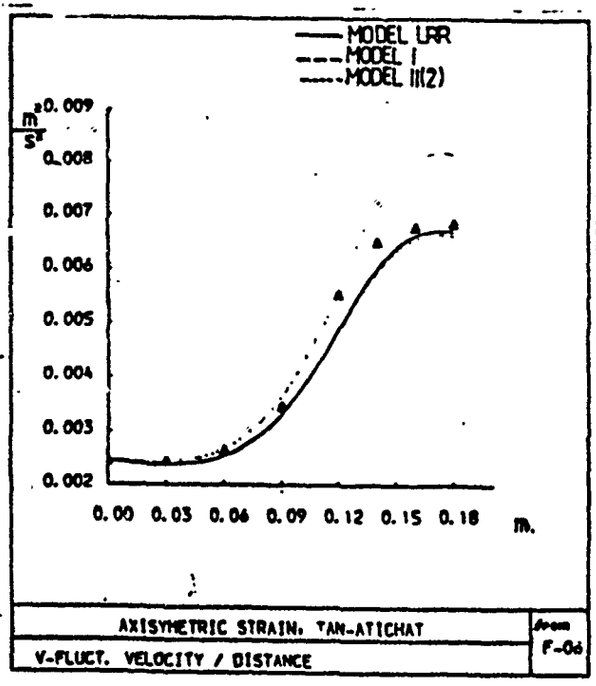
MODEL LRR
MODEL I
MODEL II(2)
m²/s²
0.009
0.008
0.007
0.006
0.005
0.004
0.003
0.002
0.00 0.03 0.06 0.09 0.12 0.15 0.18
m.
AXISYMETRIC STRAIN, TAN-ATICHAT
V-FLUCT. VELOCITY / DISTANCE
from F-06

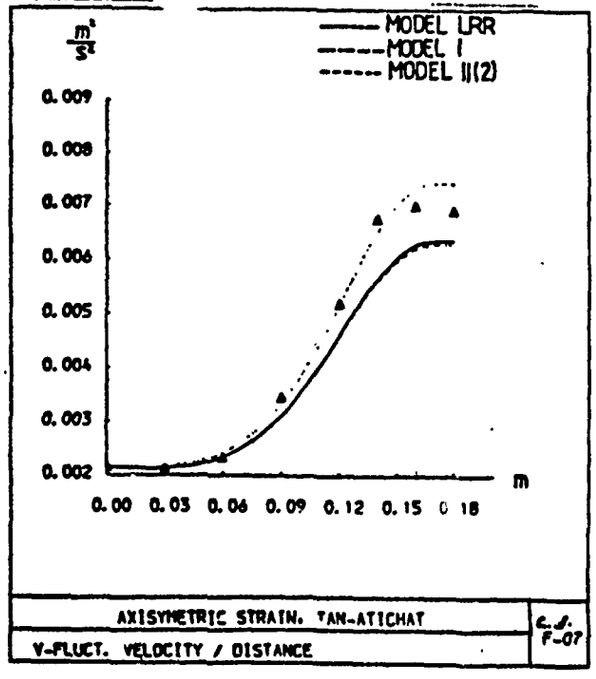
MODEL LRR
MODEL I
MODEL II(2)
m²/s²
0.009
0.008
0.007
0.006
0.005
0.004
0.003
0.002
0.00 0.03 0.06 0.09 0.12 0.15 0.18
m
AXISYMETRIC STRAIN, TAN-ATICHAT
V-FLUCT. VELOCITY / DISTANCE
F-07

Fig. F-13

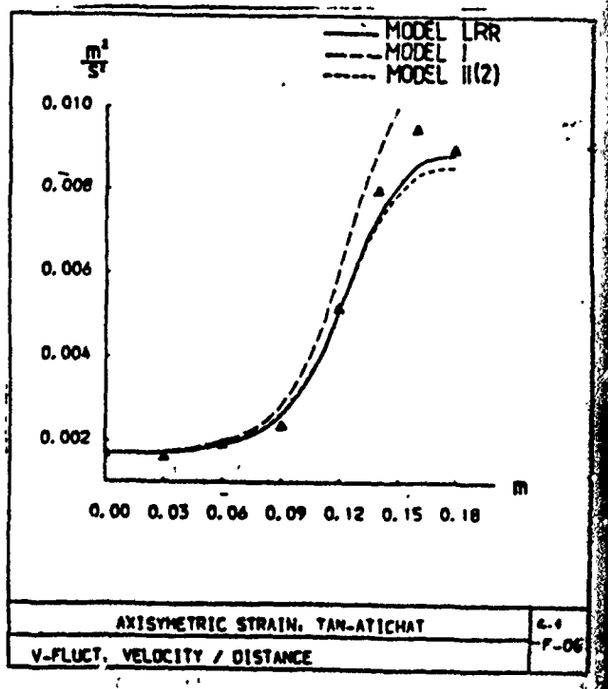
MODEL LRR
MODEL I
MODEL II(2)
m²/s²
0.010
0.008
0.006
0.004
0.002
0.00 0.03 0.06 0.09 0.12 0.15 0.18
m
AXISYMETRIC STRAIN, TAN-ATICHAT
V-FLUCT. VELOCITY / DISTANCE
F-06

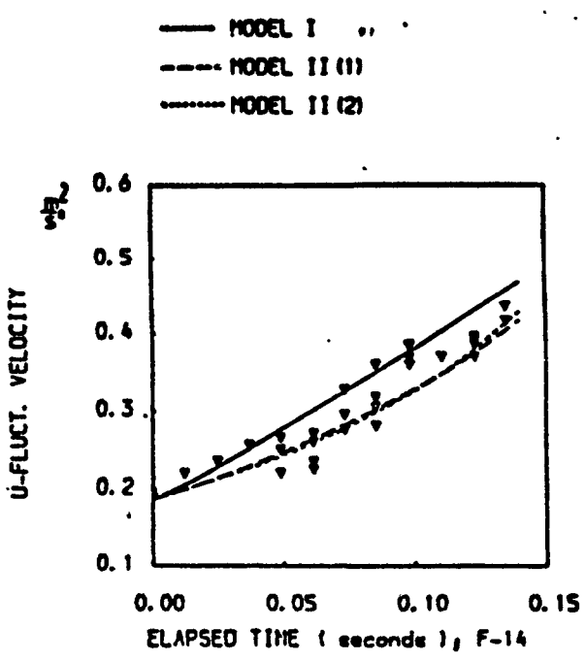
MODEL I
MODEL II (1)
MODEL II (2)
U-FLUCT. VELOCITY
0.6
0.5
0.4
0.3
0.2
0.1
0.00
0.05
0.10
0.15
ELAPSED TIME (seconds), F-14

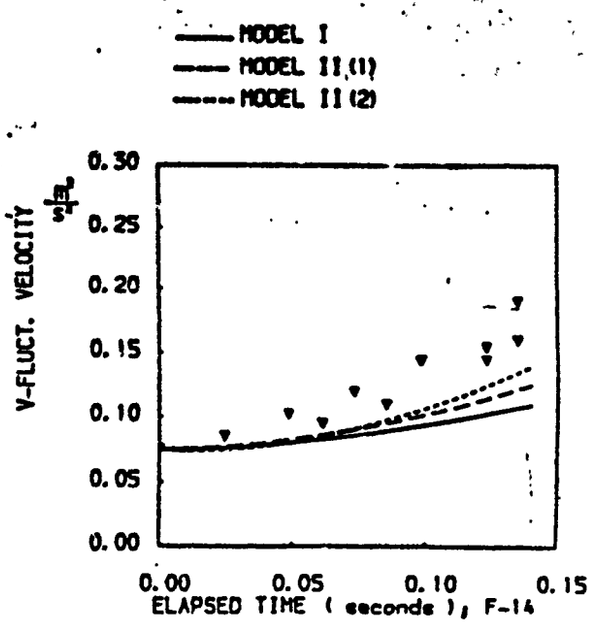
MODEL I
MODEL II (1)
MODEL II (2)
V-FLUCT. VELOCITY
0.30
0.25
0.20
0.15
0.10
0.05
0.00
0.00
0.05
0.10
0.15
ELAPSED TIME (seconds), F-14

Fig. F-14

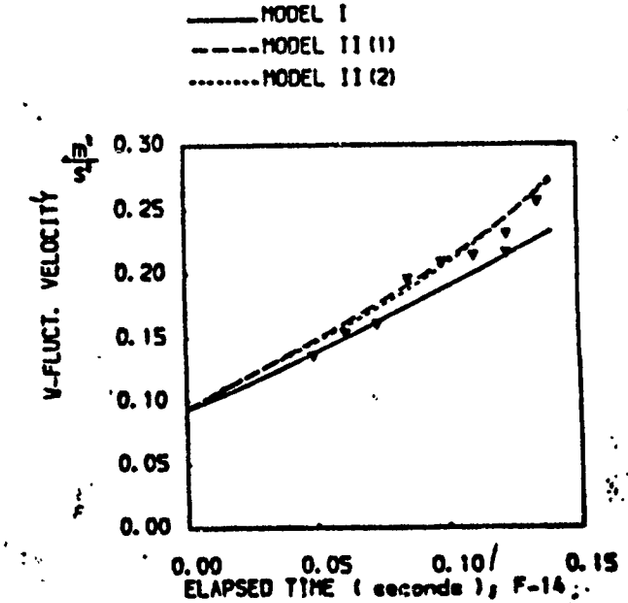
MODEL I
MODEL II (1)
MODEL II (2)
V-FLUCT. VELOCITY
0.30
0.25
0.20
0.15
0.10
0.05
0.00
0.00
0.05
0.10
0.15
ELAPSED TIME (seconds), F-14

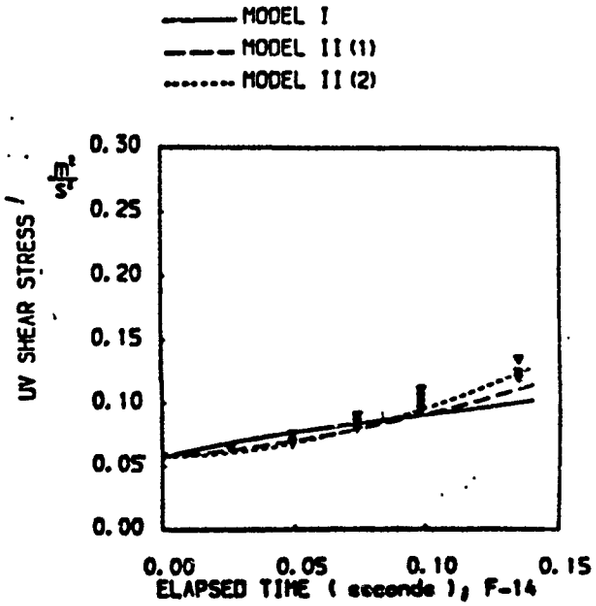
MODEL I
MODEL II (1)
MODEL II (2)
UV SHEAR STRESS
0.30
0.25
0.20
0.15
0.10
0.05
0.00
0.00
0.05
0.10
0.15
ELAPSED TIME (seconds), F-14

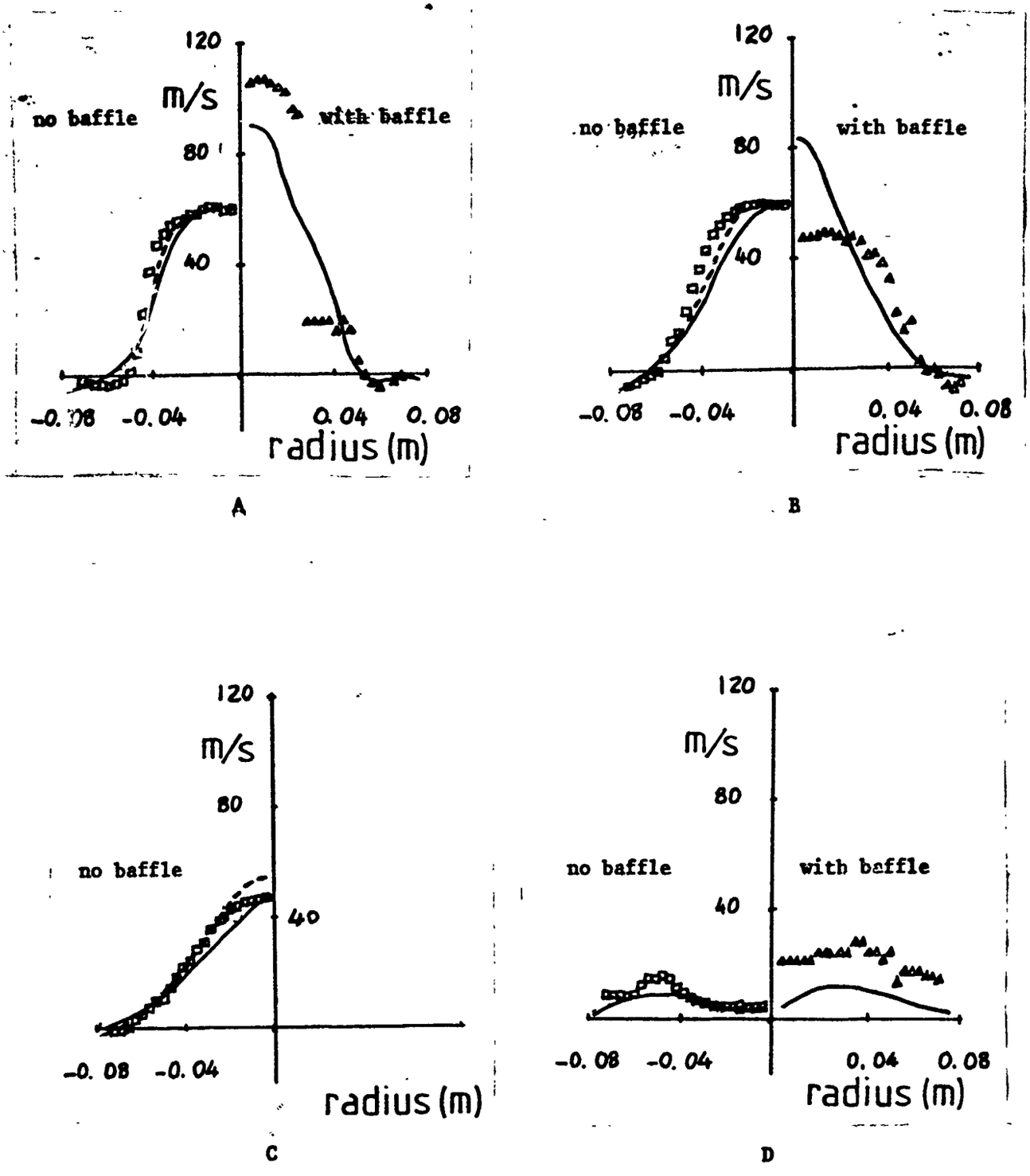

FIGURE 15 Radial variation of axial velocity with and without baffle stabiliser situated at the dump plane. A) 50 mm from the dump, B) 150 mm from the dump, C) 330 mm from the dump. D) Radial variation of rms turbulence at 150 mm from the dump plane with and without baffle.
□ and Δ are experimental points, _____ are calculated with coarse grid, ------ are calculated with fine grid.

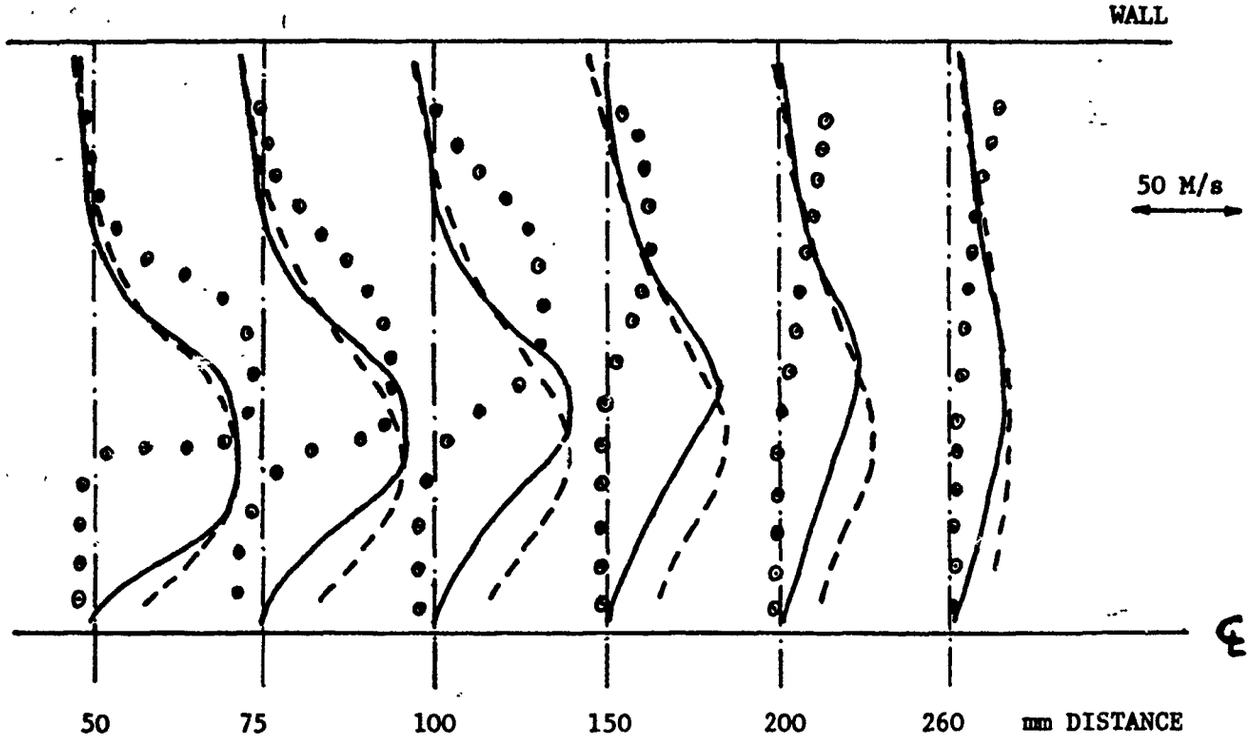

FIGURE 16 Radial variation of axial velocity at several stations from the dump plane with approximate free vortex swirler. ⊙ are experimental points, ------ are calculated using k - ε model of turbulence, ———— are calculated using the algebraic model of turbulence.

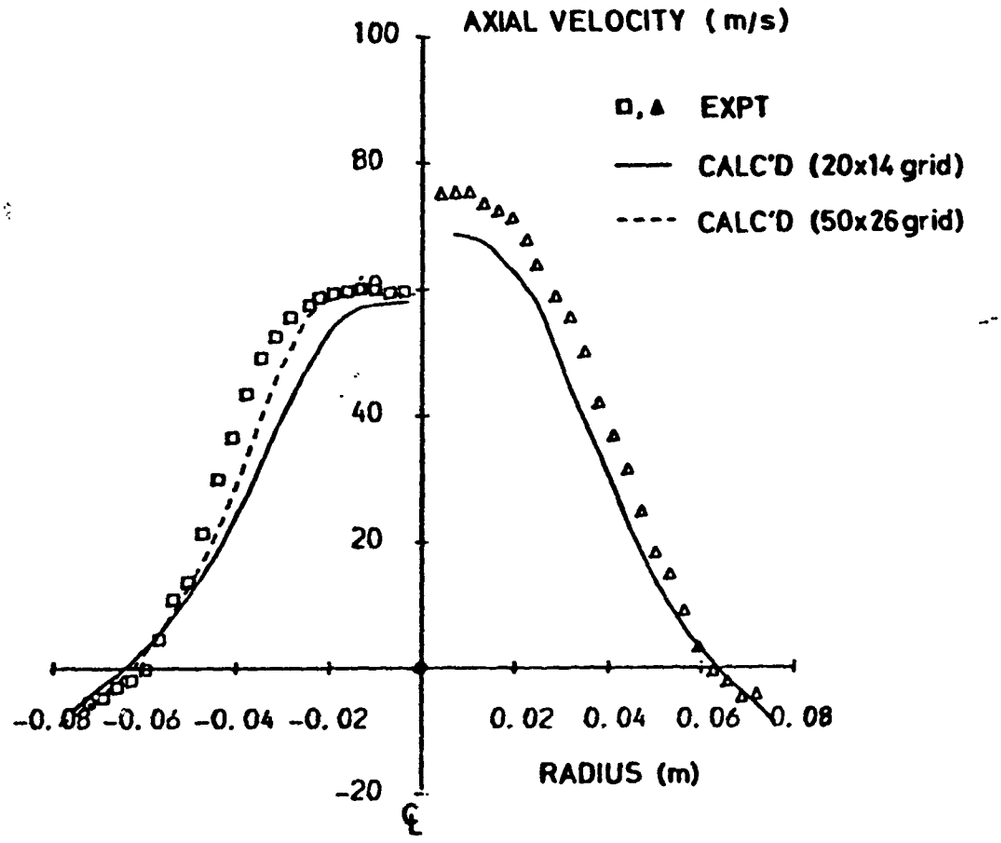

FIGURE 17 Radial variation of axial velocity at 150 mm from the dump plane with and without baffle stabiliser. In this case the baffle is situated at 8 cm upstream of the dump plane.
□ and Δ are experimental points; ——— are calculated with a coarse grid, ------ are calculated with a fine grid.

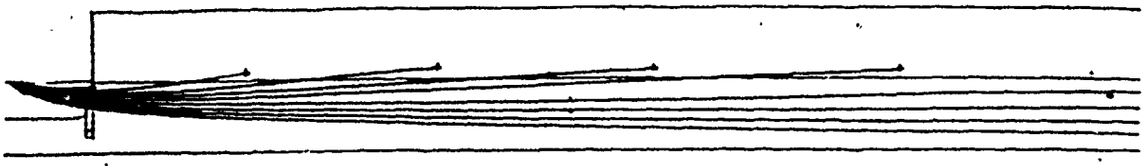

FIGURE 18 Trajectory patterns for a range of drop sizes from 5 to 100 microns. Crosses show points of evaporation

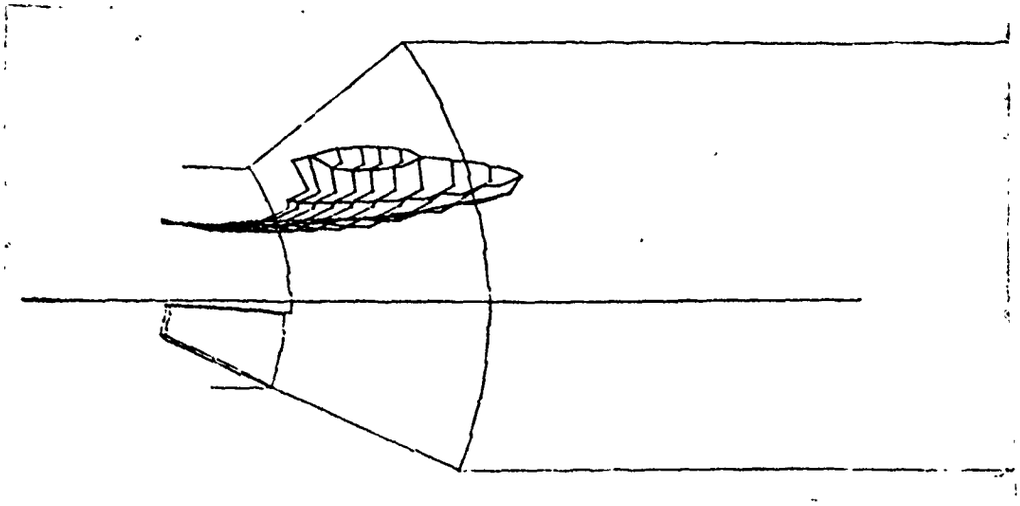

FIGURE 19 Three dimensional plot of constant mass fraction of evaporated fuel at mas fraction of 0.01.

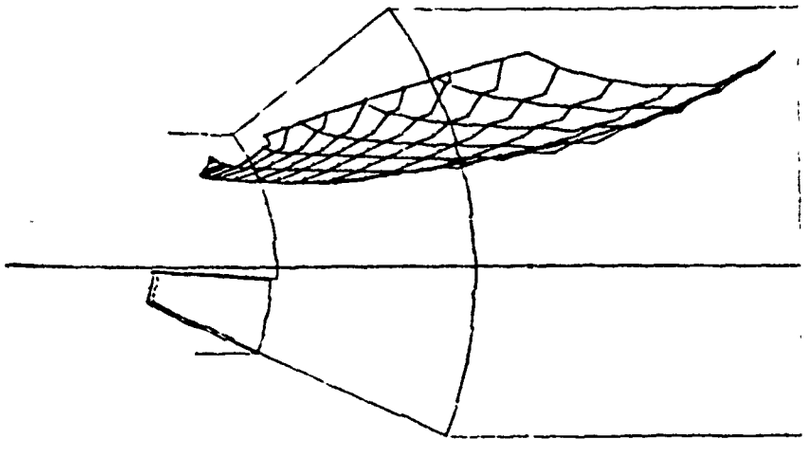

FIGURE 20 Three dimensional plot of constant temperature of 2000^{o}K.